Article

Immunity

Adoptive T Cell Therapy Targeting Different Gene Products Reveals Diverse and Context-Dependent Immune Evasion in Melanoma

Graphical Abstract

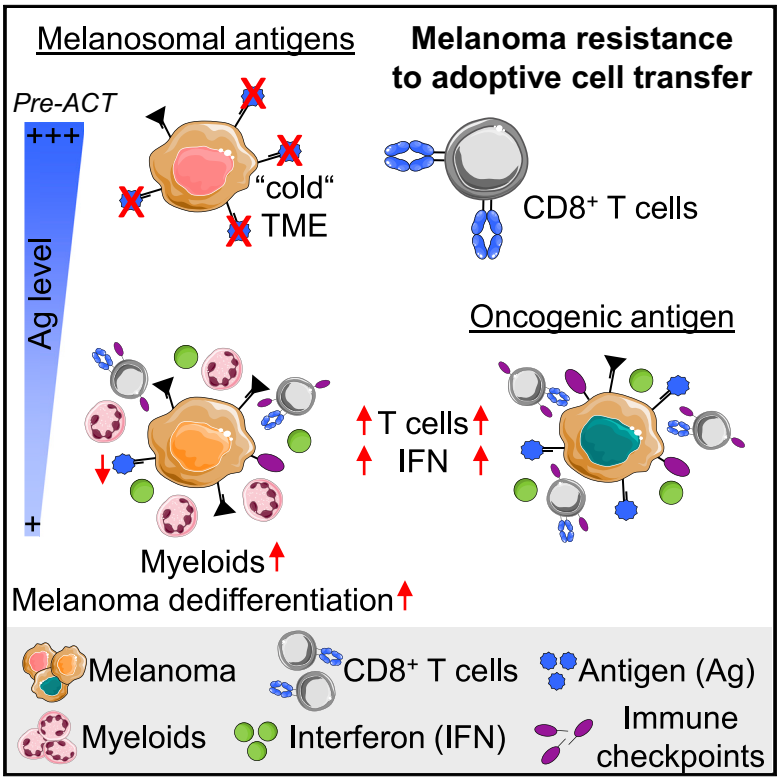

Highlights

- Comparison of different endogenous target antigens for adoptive T cell therapy
- Melanoma immune escape phenotype determined by class and level of target antigen
- Targeting melanosomal antigens drives dedifferentiation and myeloid infiltration
- Persistence of oncogenic antigen allows for salvage immune checkpoint therapy

Authors

Maike Effern, Nicole Glodde, Matthias Braun, ..., Tobias Bald, Thomas Gebhardt, Michael Hölzel

Correspondence

michael.hoelzel@ukbonn.de

In Brief

Using mouse models of melanoma, Effern et al. demonstrate how the choice of target antigens for adoptive T cell therapy determines resistance mechanisms. Targeting melanosomal antigens promotes decreased antigen expression through melanoma dedifferentiation with myeloid cell infiltration, whereas targeting oncogenic $CDK4^{R24C}$ results in antigen persistence, allowing for salvage immune checkpoint therapy.

Effern et al., 2020, Immunity *53*, 564–580
September 15, 2020
https://doi.org/10.1016/j.immuni.2020.07.007

CellPress

CellPress

Immunity

Article

Adoptive T Cell Therapy Targeting Different Gene Products Reveals Diverse and Context-Dependent Immune Evasion in Melanoma

Maike Effern,[1,2,11] Nicole Glodde,[1,11] Matthias Braun,[3,4] Jana Liebing,[1] Helena N. Boll,[1] Michelle Yong,[1] Emma Bawden,[1,2] Daniel Hinze,[1] Debby van den Boorn-Konijnenberg,[1] Mila Daoud,[1,10] Pia Aymans,[5] Jennifer Landsberg,[5] Mark J. Smyth,[4,6] Lukas Flatz,[7,8] Thomas Tüting,[9] Tobias Bald,[3] Thomas Gebhardt,[2] and Michael Hölzel[1,12,*]

[1]Institute of Experimental Oncology (IEO), Medical Faculty, University Hospital Bonn, University of Bonn, Bonn 53105, Germany
[2]Department of Microbiology & Immunology, The University of Melbourne at the Peter Doherty Institute for Infection & Immunity, Melbourne, VIC, Australia
[3]Oncology and Cellular Immunology Laboratory, QIMR Berghofer Medical Research Institute, Herston, QLD 4006, Australia
[4]Immunology in Cancer and Infection Laboratory, QIMR Berghofer Medical Research Institute, Herston, QLD 4006, Australia
[5]Laboratory of Experimental Dermatology, Department of Dermatology and Allergy, University of Bonn, Bonn 53105, Germany
[6]School of Medicine, The University of Queensland, Herston, QLD 4006, Australia
[7]Institute of Immunobiology, Kantonsspital St. Gallen, St. Gallen 9007, Switzerland
[8]Department of Dermatology, Allergology and Venerology, Kantonsspital St. Gallen, St. Gallen 9007, Switzerland
[9]Laboratory of Experimental Dermatology, Department of Dermatology, University of Magdeburg, Magdeburg, Germany
[10]Present address: Institute for Medical Microbiology, Immunology and Hygiene, Centre for Molecular Medicine Cologne, and Cologne Excellence Cluster on Cellular Stress Responses in Ageing-Associated Diseases, University of Cologne, Cologne, Germany
[11]These authors contributed equally
[12]Lead Contact
*Correspondence: michael.hoelzel@ukbonn.de
https://doi.org/10.1016/j.immuni.2020.07.007

SUMMARY

Tumor immune escape limits durable responses to T cell therapy. Here, we examined how regulation and function of gene products that provide the target epitopes for CD8$^+$ T cell anti-tumor immunity influence therapeutic efficacy and resistance. We used a CRISPR-Cas9-based method (CRISPitope) in syngeneic melanoma models to fuse the same model CD8$^+$ T cell epitope to the C-termini of different endogenous gene products. Targeting melanosomal proteins or oncogenic CDK4^{R24C} (Cyclin-dependent kinase 4) by adoptive cell transfer (ACT) of the same epitope-specific CD8$^+$ T cells revealed diverse genetic and non-genetic immune escape mechanisms. ACT directed against melanosomal proteins, but not CDK4^{R24C}, promoted melanoma dedifferentiation, and increased myeloid cell infiltration. CDK4^{R24C} antigen persistence was associated with an interferon-high and T-cell-rich tumor microenvironment, allowing for immune checkpoint inhibition as salvage therapy. Thus, the choice of target antigen determines the phenotype and immune contexture of recurrent melanomas, with implications to the design of cancer immunotherapies.

INTRODUCTION

Autologous CD8$^+$ T cells from cancer patients can be engineered to express T cell receptors (TCRs) that recognize specific peptide epitopes derived from tumor-cell-encoded antigens. Adoptive transfer of these CD8$^+$ T cells is a treatment strategy to eliminate tumor cells that present these epitopes on major histocompatibility complex (MHC) class I molecules (Rosenberg and Restifo, 2015). Choosing the right target epitope(s) represents a critical step in the development of effective adoptive T cell therapies (ACTs). Antigen expression level and epitope binding affinity to MHC class I molecules influence ACT efficacy in experimental models (Engels et al., 2013; Leisegang et al., 2016). How other variables of antigen biology impact responsiveness and resistance to ACT is poorly understood.

ACT targeting melanosomal proteins, the most typical melanocyte differentiation antigens (MDAs), have been evaluated in melanoma patients with variable success (Chandran et al., 2015; Chodon et al., 2014). Using mouse models, we have previously shown that melanomas resist MDA-directed ACT by inflammation-induced dedifferentiation (Landsberg et al., 2012), a mechanism recently confirmed in a melanoma patient (Mehta et al., 2018). In this situation, ACT-induced microenvironmental inflammation results in decreased expression of MDAs, including the one targeted by the adoptively transferred T cells. This also impairs immune recognition of melanoma cells presumably driving immune escape. Additionally, melanoma cells

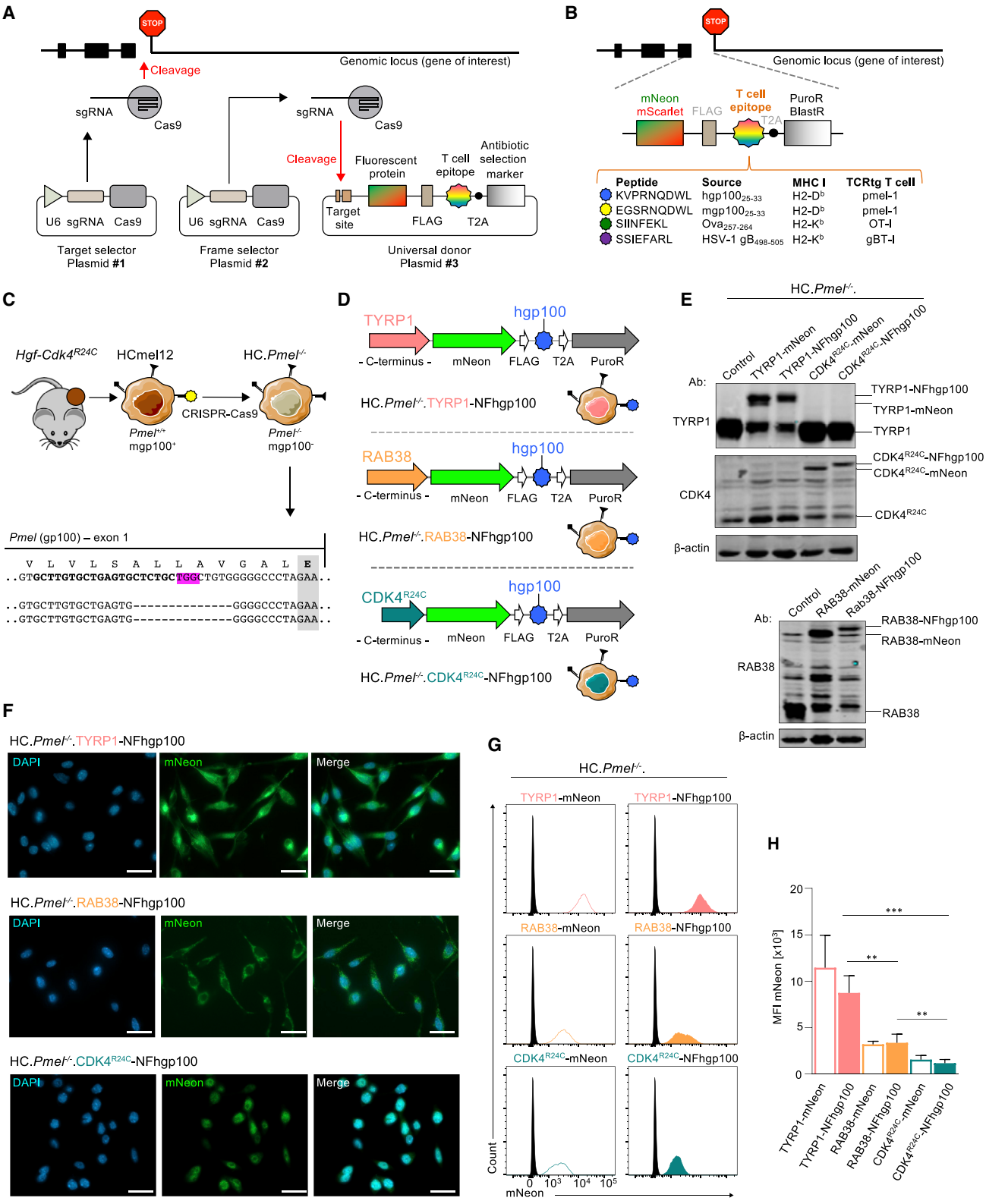

Figure 1. CRISPR-Cas9-Based Method (CRISPitope) to Fuse Model CD8+ T Cell Epitopes to Different Endogenous Gene Products in Melanoma Cells

(A) Graphical depiction of CRISPitope method.

(B) Modularity of universal donor plasmids depicting different CD8+ T cell epitopes and their MHC class I restrictions.

(legend continued on next page)

acquire neural crest progenitor-like and mesenchymal-like traits (Landsberg et al., 2012; Reinhardt et al., 2017; Riesenberg et al., 2015), a process known as "melanoma phenotype switching" (Hoek et al., 2008; Verfaillie et al., 2015).

Melanoma cells can decrease expression of non-essential MDAs, raising the question of the suitability of these antigens as targets for ACT. Epitopes derived from constitutively expressed genes, preferably essential for cell survival, may be better candidates for ACT (Anders et al., 2011; Tran et al., 2016). One such gene is a mutation of *CDK4*, encoding cyclin-dependent kinase 4; epitopes derived from $CDK4^{R24C}$ were targeted by endogenous $CD8^+$ T cells in a patient with metastatic melanoma (Wölfel et al., 1995). The mutation is oncogenic, as it blocks the interaction of $CDK4^{R24C}$ with the cell cycle inhibitor $p16^{INK4a}$ preventing cell cycle arrest. Recognition of $CDK4^{R24C}$ mutant human melanoma cells by autologous $CDK4^{R24C}$-specific T cells *in vitro* is unaffected by phenotype switching, whereas recognition by autologous MDA-specific T cells is reduced (Landsberg et al., 2012).

Even though the *in vivo* relevance of this finding remains unclear, it suggests that ACT immune escape mechanisms also depend on the regulation and function of the gene products that provide target epitopes for tumor-specific T cells. However, it is difficult to investigate T cell responses to different gene products because many variables such as different peptide-MHC binding affinities compromise comparability. As a solution, we devised a CRISPR-Cas9-based approach (CRISPitope) to fuse the same model $CD8^+$ T cell epitope to the C-termini of endogenous gene products in tumor cells. This enabled us to target endogenously encoded melanosomal TYRP1, RAB38, and oncogenic $CDK4^{R24C}$, representing two major types of melanoma antigens, with the same epitope-specific TCR-transgenic (TCRtg) $CD8^+$ T cells in syngeneic mouse melanomas. Our findings, using this "epitope-standardized" ACT (esACT) approach, suggest that the type of target antigen determines the phenotype and immune cell composition of recurrent melanomas.

RESULTS

Fusing Model T Cell Epitopes to Endogenous Gene Products in Melanoma Cells

We exploited CRISPR-assisted insertion tagging (CRISPaint) to fuse model T cell epitopes to the C-termini of endogenous gene products in melanoma cells (Schmid-Burgk et al., 2016). Briefly, a gene-specific single guide RNA (sgRNA) recruits Cas9 endonuclease, which introduces a double-strand break upstream of the stop codon of the gene of interest. A second sgRNA directs the cut of a co-transfected universal donor plasmid taking reading frames into account. The cleaved universal donor DNA then integrates at the site of the double-strand break via non-homologous end-joining and creates C-terminal gene fusions with tags of choice. For our aim, we designed universal donor plasmids encoding tags with the following core structure: fluorescent protein (e.g., mNeon)–FLAG-tag–T cell epitope–T2A proteolytic cleavage site–antibiotic selection marker (Figure 1A). This design allowed for visualization, fluorescent cell sorting, detection by western blot, recognition by epitope-specific T cells, and selection by antibiotics. We generated several universal donor plasmids with different $CD8^+$ T cell epitopes (e.g., human $gp100_{25\text{-}33}$) (Figure 1B). For simplicity, we termed our approach CRISPR-assisted insertion of epitopes (CRISPitope), offering flexibility with regard to peptide affinities, MHC class I restriction, and TCRtg T cells.

For our project, we decided to use HCmel12 mouse melanoma cells derived from a serial transplant of a primary melanoma in *Hgf-Cdk4*^{R24C} mice (Bald et al., 2014a). HCmel12 is homozygous for mutant *Cdk4*^{R24C} and expresses typical MDAs under the control of MITF, the master melanocyte lineage transcription factor (Goding and Arnheiter, 2019). Using CRISPR-Cas9, we ablated the melanosomal antigen *Pmel* (premelanosome protein, also known as gp100) and established a monoclonal *Pmel*$^{-/-}$ cell line (HC.*Pmel*$^{-/-}$) (Figure 1C). Human gp100 (hgp100) is a high-affinity epitope that is strongly recognized by $CD8^+$ TCRtg pmel-1 T cells. In contrast, the low-affinity mouse gp100 (mgp100) epitope is also recognized by pmel-1 T cells, but poorly (Engels et al., 2013). For our purpose, we used hgp100 as model $CD8^+$ T cell epitope, as its higher peptide-MHC affinity compared to mgp100 created a situation similar to immunogenic neoepitopes, which also have higher affinities than the wild-type epitopes (Hanada et al., 2019; Łuksza et al., 2017).

TYRP1, RAB38, and $CDK4^{R24C}$ as Model Melanosomal and Oncogenic T Cell Targets

Next, we tagged endogenous melanosomal TYRP1 (tyrosinase-related protein 1) and RAB38 (RAB38, member RAS oncogene family also known as NY-MEL-1), two typical MDAs (Kawakami et al., 1994; Walton et al., 2006), with mNeon (N), FLAG (F), and hgp100 in HC.*Pmel*$^{-/-}$ cells (Figure 1D, top and middle). We named the tag NFhgp100 and the generated gene fusion products TYRP1-NFhgp100 and RAB38-NFhgp100. After antibiotic selection, we successfully purified tagged cells based on mNeon positivity by flow cytometry. The resulting polyclonal cell lines were named HC.*Pmel*$^{-/-}$.TYRP1-NFhgp100 and HC.*Pmel*$^{-/-}$.RAB38-NFhgp100. For an oncogene product, we chose mutant $CDK4^{R24C}$ because HC.*Pmel*$^{-/-}$ cells harbor this driver mutation. As described above, we tagged $CDK4^{R24C}$ with NFhgp100 and named the generated polyclonal cell line HC.*Pmel*$^{-/-}$.$CDK4^{R24C}$-NFhgp100 (Figure 1D, bottom). For

(C) Generation and genomic characterization of Pmel (gp100)-deficient HC.*Pmel*$^{-/-}$ cells.
(D) Engineered endogenous TYRP1 (top), RAB38 (middle), and $CDK4^{R24C}$ (bottom) gene fusion products with mNeon-FLAG-hgp100 tag (NFhgp100).
(E) Western blot analysis of TYRP1 and $CDK4^{R24C}$ (top) and RAB38 (bottom) expression in CRISPitope-engineered melanoma cells.
(F) Representative epifluorescence images visualizing TYRP1-NFhgp100 (top), RAB38-NFhgp100 (middle), and $CDK4^{R24C}$-NFhgp100 (bottom) subcellular localization. Left: DAPI; middle: mNeon; right: merge. Scale bars: 20 μM.
(G and H) Representative histograms (G) and corresponding quantification (H) of mNeon expression (MFI: mean fluorescence intensity) by flow cytometry in HC.*Pmel*$^{-/-}$ cells expressing TYRP1-NFhgp100, RAB38-NFhgp100, and $CDK4^{R24C}$-NFhgp100 or respective mNeon-only control gene fusions (n = 4; mean ± SD). Statistics: ***$p < 0.001$, **$p < 0.01$; unpaired two-sided t test.
See also Figure S1.

control purposes, we also tagged TYRP1, RAB38, and CDK4^{R24C} with mNeon tags lacking the hgp100 epitope (HC.*Pmel*$^{-/-}$ mNeon-only controls). Western blotting and fluorescence microscopy confirmed increased molecular weight due to the tag and correct subcellular localization of the endogenously encoded gene fusion products, respectively (Figures 1E and 1F). To avoid single-cell cloning biases, we pursued a polyclonal cell line strategy that explained the presence of, e.g., untagged TYRP1 from heterozygous tagging (Figure 1E). As mentioned above, stringent cell sorting for mNeon positivity ensured at least one tagged allele per cell. Formally, we could not exclude the presence of untagged antigen-negative cells at very low frequency, but this was tolerated to allow for genetic heterogeneity as also observed in patients. Finally, we compared the expression level of the gene fusion products by flow cytometry (mNeon intensity) showing highest level for TYRP1-NFhgp100, whereas RAB38-NFhgp100 and CDK4^{R24C}-NFhgp100 were expressed at lower and more comparable levels (Figures 1G and 1H).

T Cell Recognition of CRISPitope-Engineered Melanoma Cells *In Vitro*

We then verified that pmel-1 T cells recognized HC.*Pmel*$^{-/-}$ cells expressing either TYRP1-NFhgp100, RAB38-NFhgp100, or CDK4^{R24C}-NFhgp100. To this end, we co-cultured the different engineered HC.*Pmel*$^{-/-}$ cells, including mNeon-only fusion controls, together with splenocytes from naive pmel-1 TCRtg mice. We monitored hgp100-dependent activation of pmel-1 T cells by induction of cell surface CD69, a well-characterized T cell activation marker (Figure 2A). Comparing all models, HC.*Pmel*$^{-/-}$ cells expressing TYRP1-NFhgp100 caused the strongest induction of CD69 on pmel-1 T cells in line with highest antigen expression (Figures 2B and 2C). Activation of pmel-1 T cells was also confirmed by enhanced production of IFN-γ and TNF-α (Figures S1A and S1B). Activation of pmel-1 T cells also required pre-stimulation of melanoma cells with IFN-γ in order to upregulate MHC class I antigen presentation. Induction of MHC class I (H2-D^{b}) surface expression by IFN-γ was comparable on all cell lines (Figures 2D and 2E). HC.*Pmel*$^{-/-}$ mNeon-only cell lines as negative controls failed to induce CD69 surface expression on pmel-1 T cells. We also tagged other MDAs including DCT, GPNMB, and SOX10 with NFhgp100, and co-culture assays confirmed pmel-1 T cell activation (Figure S1C). Thus, CRISPitope-engineered melanoma cells can model the presentation and recognition of clinically relevant tumor antigens (Bassani-Sternberg et al., 2016).

Experimental Versatility of CRISPitope Approach

In order to show versatility of the CRISPitope technique with regard to fluorescent proteins, epitopes, and cell lines, we first engineered HC.*Pmel*$^{-/-}$ cells expressing fusions of TYRP1 with red fluorescent mScarlet and either low-affinity mgp100 or high-affinity hgp100 epitopes, which confirmed stronger activation of pmel-1 T cells by the hgp100 fusion *in vitro* (Figures S1D and S1E). Next, we used ACTB (actin beta) or ACTG1 (actin gamma 1) as endogenous fusion partners, the HSV-1 gB$_{498\text{-}505}$ CD8^{+} T cell epitope, and B16 melanoma cells (Figure S1F). In co-culture assays, we monitored epitope-specific activation of gBT-I TCRtg CD8^{+} T cells, recognizing gB$_{498\text{-}505}$ in a H2-K^{b}-restricted manner, by intracellular expression of the cytokines IFN-γ and TNF-α using flow cytometry (Figures S1G and S1H) (Macleod et al., 2014). Again, T cell activation required pre-stimulation of B16 cells with IFN-γ for MHC class I induction (Figures S1I–S1K). Hence, CRISPitope is versatile and can be applied to various experimental models.

Epitope-Standardized ACT Targeting Endogenous TYRP1, RAB38, or CDK4^{R24C}

After completing the technical validation of the CRISPitope-engineered cells *in vitro*, we focused on our central aim of comparing ACT targeting melanomas that express the hgp100 epitope fused to endogenous TYRP1, RAB38, or CDK4^{R24C} in syngeneic mouse models. Our ACT protocol consists of chemotherapeutic conditioning with a single dose of cyclophosphamide, intravenous injection of gp100-specific CD90.1^{+}CD8^{+} TCRtg pmel-1 T cells, *in vivo* activation of pmel-1 T cells with a hgp100-expressing adenovirus vaccine (Ad-hgp100), and stimulation of the innate immune system with CpG and Poly(I:C) (Glodde et al., 2017; Landsberg et al., 2012). We referred to this protocol as epitope-standardized ACT (esACT) when treating CRISPitope-engineered melanoma models, because the same effector T cells targeted different endogenous gene products by a standardized model epitope. First, we verified that esACT was only effective against melanomas expressing hgp100 gene fusion products, but not mNeon-only control melanomas. We injected HC.*Pmel*$^{-/-}$ cells expressing either TYRP1-mNeon, RAB38-mNeon, or CDK4^{R24C}-mNeon into the flanks of syngeneic mice (Figures S2A–S2C). In line with absent hgp100 expression, none of the mNeon-only melanomas responded to esACT aside from transient effects by intratumor injections of CpG and Poly(I:C) (Figures S2D–S2I). Kaplan-Meier curves also confirmed similar survival regardless of esACT treatment or the model used (Figure S2J).

Next, we investigated esACT efficacy against melanomas expressing hgp100 gene fusion products. Flanks of syngeneic mice were injected with HC.*Pmel*$^{-/-}$ cells expressing either TYRP1-NFhgp100, RAB38-NFhgp100, or CDK4^{R24C}-NFhgp100 (Figures 3A–3C). Without treatment, all tumors grew progressively with similar kinetics until mice needed to be sacrificed (Figures 3D–3F). In contrast, most tumors in esACT-treated mice initially responded to therapy. With regard to cure rates, esACT against TYRP1-NFhgp100 was most effective (68%), followed by CDK4^{R24C}-NFhgp100 (52%) and RAB38-NFhgp100 (20%) (Figures 3G–3I). In remaining mice, tumor recurrences occurred over a period of two months. Kaplan-Meier plots showed better survival of esACT-treated mice bearing melanomas that expressed TYRP1-NFhgp100 compared to RAB38-NFhgp100 with CDK4^{R24C}-NFhgp100 in between (Figure 3J), whereas no differences were seen between the untreated cohorts. Using flow cytometry, we also monitored the expansion of adoptively transferred pmel-1 T cells in the peripheral blood by the congenic marker CD90.1 (Figure 3K). Frequencies of circulating pmel-1 T cells were similarly high in the TYRP1-NFhgp100 and CDK4^{R24C}-NFhgp100 groups, but lower in the RAB38-NFhgp100 group, as also observed in the mNeon-only control groups (Figures 3L, S2K, and S2L). Of note, when compared to our previously reported data (Glodde et al., 2017), all CRISPitope models expressing hgp100 gene fusion products responded

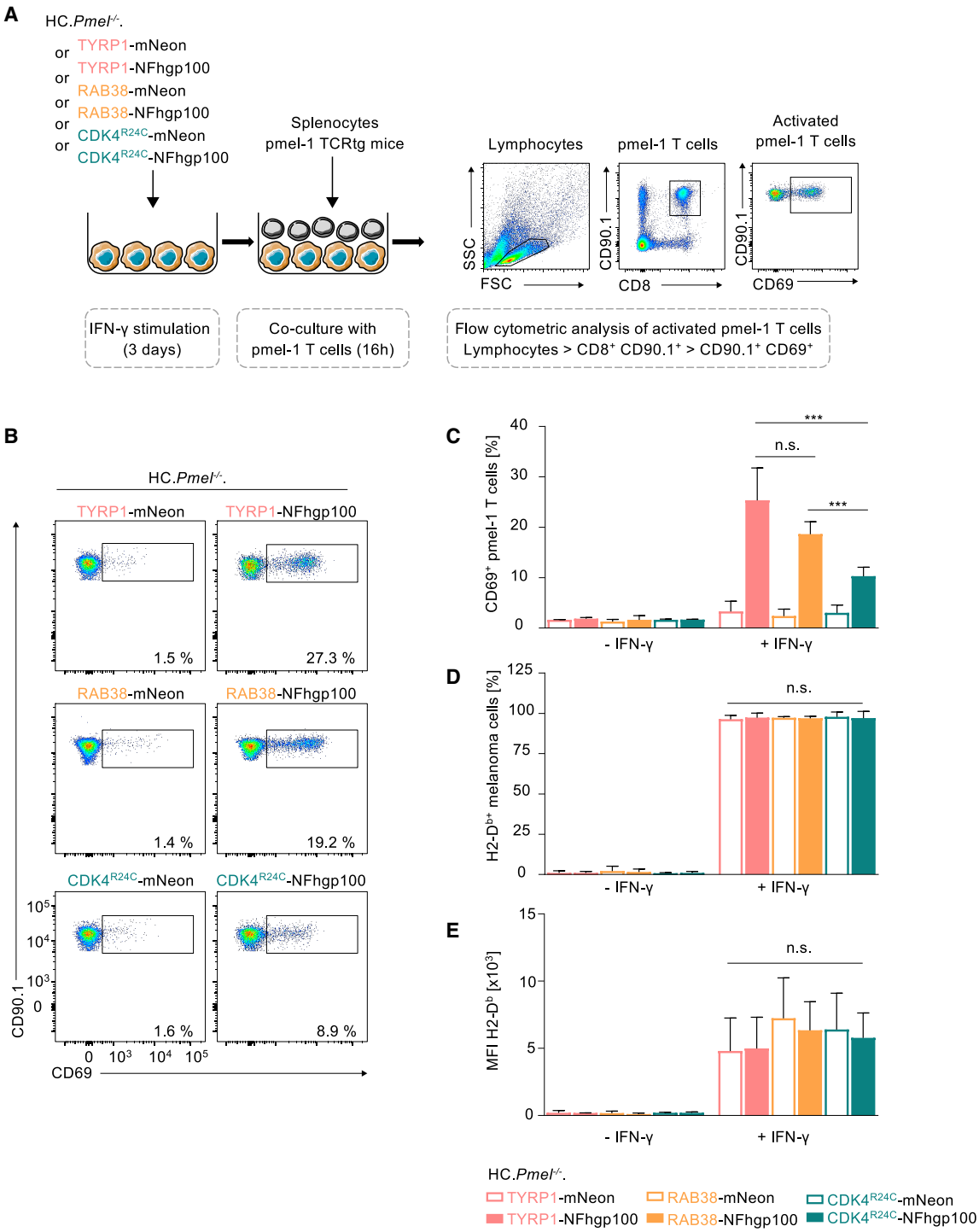

Figure 2. Recognition of CRISPitope-Engineered Melanoma Cells by the Same Epitope-Specific TCRtg CD8+ T Cells

(A) Experimental setup and gating strategy for *in vitro* pmel-1 T cell activation assay using indicated HC.*Pmel*$^{-/-}$ cells.

(B and C) Representative flow cytometric plots (B) and corresponding quantification (C) showing CD69 surface expression on CD8$^+$ CD90.1$^+$ pmel-1 T cells 16 h after co-culture with indicated HC.*Pmel*$^{-/-}$ cells ($n \geq 3$; mean ± SD). Statistics: ***$p < 0.001$; unpaired two-sided t test.

(D and E) Quantification of H2-D^b surface expression on indicated HC.*Pmel*$^{-/-}$ cells treated with IFN-γ (1000 U ml^{-1}) for 72 h shown as frequency (%) (D) and mean fluorescence intensity (MFI) (E) ($n \geq 3$; mean ± SD). Statistics: n.s.: not significant; Mann-Whitney test.

See also Figure S1.

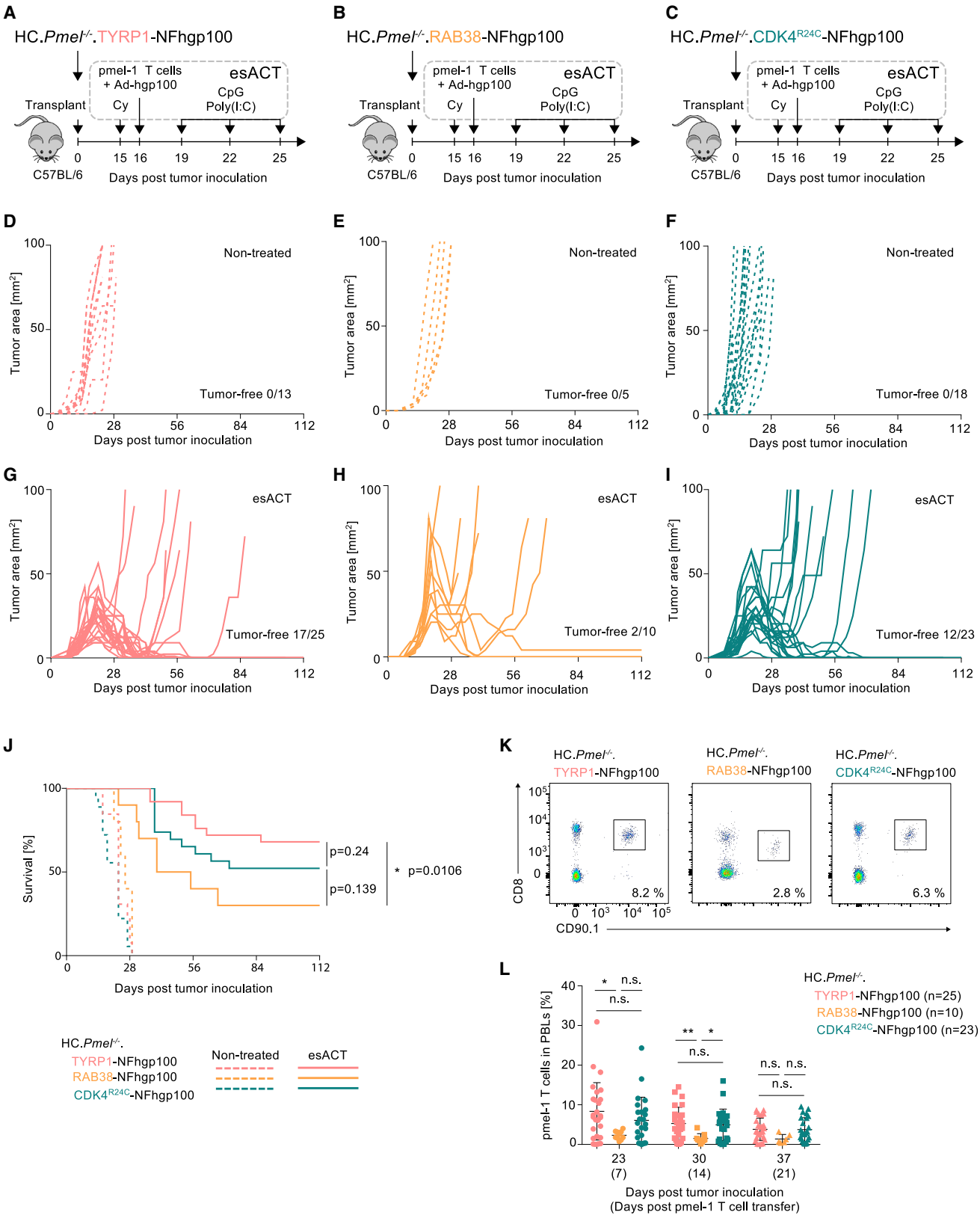

(legend on next page)

better to esACT than parental HCmel12 melanomas, in which the low-affinity mgp100 epitope is produced from endogenous PMEL protein (Figures S2M–S2O). Phenotypically, the HC.*Pmel*$^{-/-}$ founder clone and all therefrom derived CRISPitope models highly expressed melanocyte lineage and MITF target genes just as well as parental HCmel12 when compared to a well-characterized dedifferentiated MITF^{low} melanoma (Figure S2P) (Riesenberg et al., 2015).

Furthermore, we asked how Ad-hgp100 vaccination influenced therapeutic efficacy, assuming that a strong systemic immune response by Ad-hgp100 homogenized immune responses against the different hgp100 gene fusion products. In other words, we reasoned that Ad-hgp100 reduced the requirement for high antigen expression by melanoma cells in order to boost pmel-1 T cell expansion early during treatment. Therefore, we omitted Ad-hgp100 from the esACT protocol and treated mice bearing TYPR1-NFhgp100 and CDK4^{R24C}-NFhgp100 melanomas (Figures S3A and S3B), as these two models differed the most in antigen level (Figures 1G and 1H). Omitting Ad-hgp100 profoundly reduced survival of mice with CDK4^{R24C}-NFhgp100 melanomas (0% cure rate), whereas 26% of mice within the TYPR1-NFhgp100 cohort still achieved long-term remissions (Figures S3C– S3E). This result corroborated that Ad-hgp100 was critical for effective esACT if antigen expression by melanoma cells was less abundant.

Diverse Mechanisms of Antigen Loss in esACT-Recurrent Melanomas

Next, we investigated if antigen loss occurred as immune evasion mechanism in esACT-recurrent (R) melanomas. Antigen transcript level of *Tyrp1-NFhgp100*, *Rab38-NFhgp100*, and *Cdk4*^{R24C}*-NFhgp100* were assessed by 3′mRNA-seq (3' messenger RNA sequencing) (Figures 4A–4C). Presence and integrity of NFhgp100-tags (CRISPitope cassette) in the genomic DNA were determined by a PCR-based approach and sequencing (Figure S4). Antigen protein level was determined by flow cytometry (mNeon intensity) as summarized in Figures 4A–4C. Decreased antigen expression was frequent in recurrent TYRP1-NFhgp100 and RAB38-NFhgp100 melanomas, but not in recurrent CDK4^{R24C}-NFhgp100 melanomas. In the case of TYRP1-NFhgp100, recurrent melanomas R1, R4, and R8 lacked the NFhgp100-tag (CRISPitope cassette) in the genomic DNA, consistent with loss of mRNA and mNeon expression (Figures 4A and 4D). R3 showed a truncating mutation upstream of the hgp100 tag in the mNeon open-reading frame that abrogated antigen expression (Figures 4D and S4B). R2 showed transcriptional silencing of *Tyrp1-NFhgp100*, which was selective to the tagged allele, as untagged TYRP1 was detectable by western blot (Figure 4E). R5, R6, and R7 showed reduced mNeon signals (Figures 4A and 4D; R5 shown exemplarily), somewhat lower than expected from transcript level, suggestive of post-transcriptional regulation. In recurrent RAB38-NFhgp100 melanomas, low mRNA expression correlated with low mNeon signals, but none of the cases were negative for the NFhgp100 tag in the genomic DNA (Figures 4B, 4F, and S4C). The only recurrent CDK4^{R24C}-NFhgp100 melanoma (R10) showing antigen loss also lacked the NFhgp100 tag in the genomic DNA (Figures 4C, 4G, and S4D). Taken together, decreased antigen expression or loss was common if esACT was directed against the melanosomal targets TYRP1 or RAB38, but not oncogenic CDK4^{R24C}. Half of the recurrent TYRP1-NFhgp100 melanomas showed hardwired genomic antigen loss (R1, R3, R4, and R8), but none of the recurrent RAB38-NFhgp100 melanomas. This was likely due to lower antigen expression and thus a lower immune selection pressure in the latter. All cases with hardwired genomic antigen loss recurred after complete regression (CR: minimal tumor area $\leq$1 mm^2), suggestive of clonal outgrowth (Figure 4A).

esACT Targeting Melanosomal Antigens Enforces Melanoma Phenotype Switching

We reasoned that the RAB38-NFhgp100 and CDK4^{R24C}-NFhgp100 models were best suited for comparing immune evasion mechanisms with regard to different antigen biology as baseline antigen expression was comparable. Given that decreased antigen expression was prominent in recurrent RAB38-NFhgp100 melanomas, but there was no evidence for genomic hardwired loss, we suspected melanoma dedifferentiation as the underlying mechanism (Landsberg et al., 2012; Mehta et al., 2018; Riesenberg et al., 2015). Transcriptome analyses revealed that melanocyte lineage genes, which are involved in pigment production, and other typical MITF target genes were decreased in recurrent RAB38-NFhgp100 melanomas (Figures 5A and 5B). Intriguingly, expression of these genes was unaltered in recurrent CDK4^{R24C}-NFhgp100 melanomas, revealing a profound difference between the two models (Figures 5A and 5B). To corroborate this finding, we performed gene set enrichment analysis (GSEA) using the MSigDB hallmark collection with added melanoma phenotype signatures (Liberzon et al., 2015; Subramanian et al., 2005). Melanoma dedifferentiation is associated with a mesenchymal-like cell state transition also termed as an "invasive" phenotype (Hoek et al., 2008;

Figure 3. Epitope-Standardized Adoptive T Cell Therapy (esACT) Targeting Endogenous TYPR1, RAB38, or CDK4^{R24C}

(A–C) Experimental setup of esACT targeting TYRP1-NFhgp100 (A), RAB38-NFhgp100 (B), and CDK4^{R24C}-NFhgp100 (C) in respectively engineered HC.*Pmel*$^{-/-}$ syngeneic melanomas (Cy: cyclophosphamide; Ad-hgp100: hgp100-expressing adenovirus; CpG and Poly(I:C): innate immune ligands).

(D–F) Individual tumor growth curves (tumor area in mm^2) of untreated HC.*Pmel*$^{-/-}$.TYRP-NFhgp100 (D), HC.*Pmel*$^{-/-}$.RAB38-NFhgp100 (E), and HC.*Pmel*$^{-/-}$.CDK4^{R24C}-NFhgp100 (F) melanomas. Cohort sizes as indicated.

(G–I) Individual tumor growth curves (tumor area in mm^2) of esACT-treated HC.*Pmel*$^{-/-}$.TYRP-NFhgp100 (G), HC.*Pmel*$^{-/-}$.RAB38-NFhgp100 (H), and HC.*Pmel*$^{-/-}$.CDK4^{R24C}-NFhgp100 (I) melanomas. Cohort sizes as indicated.

(J) Kaplan-Meier survival curves of non-treated or esACT-treated cohorts as indicated. Statistics: p values indicated in graph; log-rank test.

(K) Representative flow cytometric plots showing CD8$^+$ CD90.1$^+$ pmel-1 T cells 7 days after adoptive transfer in the peripheral blood of mice bearing HC.*Pmel*$^{-/-}$ melanomas as indicated.

(L) Quantification of CD8$^+$ CD90.1$^+$ pmel-1 T cells in the peripheral blood 7, 14, and 21 days after adoptive transfer in individual mice bearing HC.*Pmel*$^{-/-}$ melanomas and numbers as indicated. Statistics: $^{**}p < 0.01$, $^{*}p < 0.05$, n.s.: not significant; Mann-Whitney-test.

See also Figures S2 and S3.

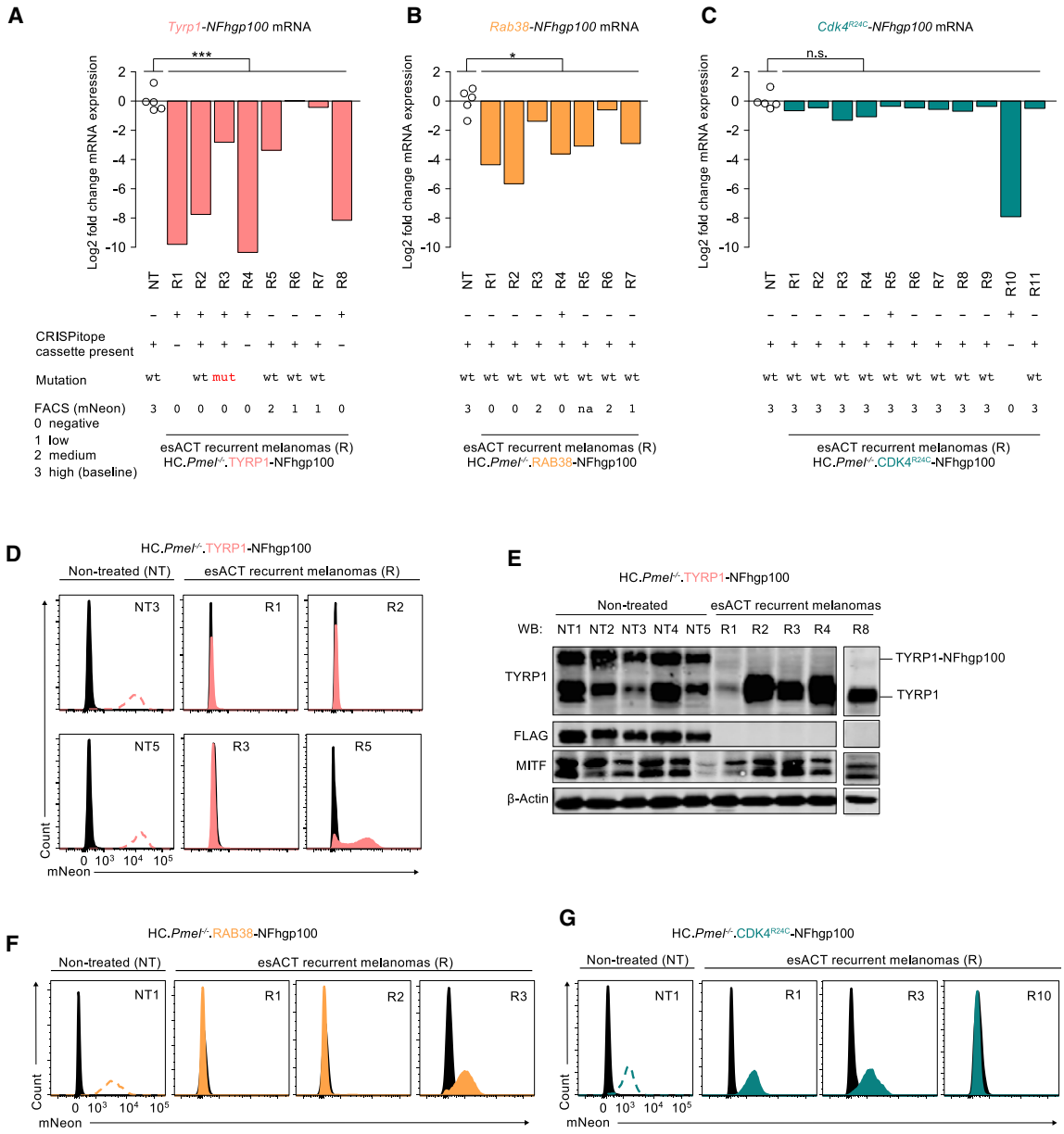

Figure 4. Diverse Mechanisms of Antigen Loss in esACT-Recurrent Melanomas

(A–C) *TYRP1-NFhgp100* (A), *RAB38-NFhgp100* (B), and *CDK4*^{R24C}*-NFhgp100* (C) mRNA expression by RNA-seq (log2 fold change) in indicated non-treated (NT) and esACT-recurrent HC.*Pmel*$^{-/-}$ melanomas. Additional depiction of complete regression status (minimal tumor area $\leq$ 1 mm^2), presence, and mutations status of CRISPitope cassette (NFhgp100 tag) in genomic DNA and mNeon expression assessed by flow cytometry. Statistics: ***FDR < 0.001; *FDR < 0.05, n.s.: not significant; unpaired two-sided t test.

(D) Histograms exemplarily showing mNeon expression by flow cytometry in non-treated (NT) and recurrent (R) HC.*Pmel*$^{-/-}$.TYRP1-NFhgp100 melanomas.

(E) Western blot analysis of TYRP1, FLAG, MITF, and β-Actin from non-treated (NT) and recurrent (R) HC.*Pmel*$^{-/-}$.TYRP1-NFhgp100 melanomas with antigen loss (R1-4, R8).

(F and G) Histograms exemplarily showing mNeon expression by flow cytometry in non-treated (NT) and recurrent (R) HC.*Pmel*$^{-/-}$.RAB38-NFhgp100 (F) and HC.*Pmel*$^{-/-}$.CDK4^{R24C}-NFhgp100 (G) melanomas.

See also Figure S4.

Riesenberg et al., 2015; Verfaillie et al., 2015). Compared to non-treated controls or recurrent CDK4^{R24C}-NFhgp100 melanomas, the invasive phenotype signature by Verfaille et al. was significantly enriched in recurrent RAB38-NFhgp100 melanomas (Figures 5C and 5D). This was also true for the three recurrent TYRP1-NFhgp100 melanomas in which antigen expression was not completely lost (R5-7) (Figure 5E). Consistently, the expression of *Axl*, one of the best characterized markers for invasive melanomas (Müller et al., 2014), was highest in RAB38-NFhgp100- and the aforementioned TYRP1-NFhgp100- (R5-7)

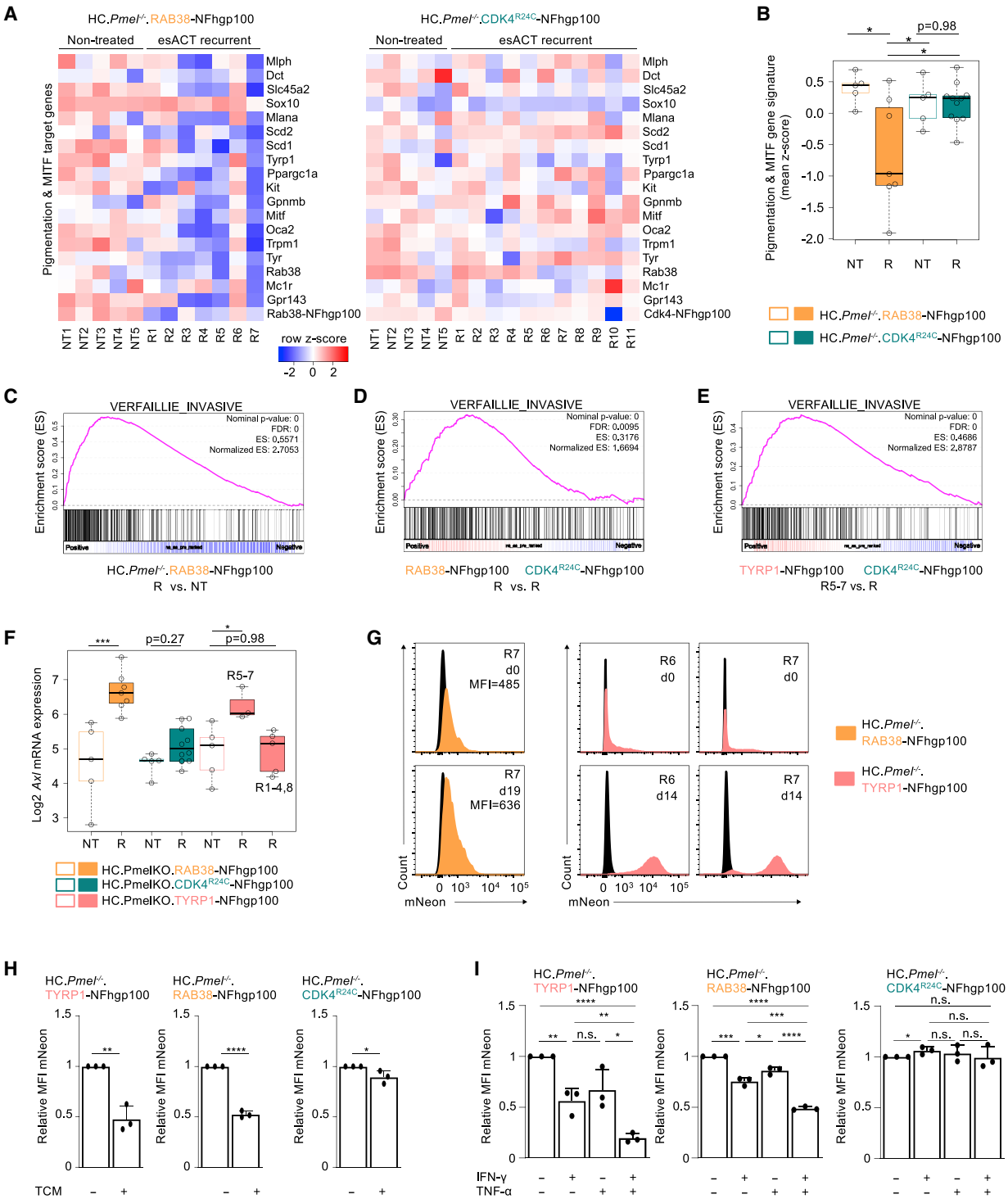

Figure 5. Dedifferentiation and Mesenchymal-like Phenotype Switching of Recurrent Melanomas Promoted by esACT Targeting Melanosomal Proteins, but Not CDK4^{R24C}

(A and B) Heatmap visualization (A) and quantification (B) of expression of pigmentation and MITF target gene signature in indicated conditions. NT: non-treated; R: esACT-recurrent melanoma. Statistics: *FDR < 0.05, two-sided t test.

(C) GSEA plots for Verfaillie invasive signature comparing recurrent (R) and non-treated (NT) HC.*Pmel*$^{-/-}$.RAB38-NFhgp100 melanomas. FDR: false discovery rate, ES: enrichment score.

(D) GSEA plots for Verfaillie invasive signature comparing recurrent (R) HC.*Pmel*$^{-/-}$.RAB38-NFhgp100 and recurrent (R) HC.*Pmel*$^{-/-}$.CDK4^{R24C}-NFhgp100 melanomas. FDR: false discovery rate, ES: enrichment score.

(legend continued on next page)

recurrent melanomas (Figure 5F). In sum, recurrent melanomas showed a dedifferentiated invasive phenotype switch if T cells were directed against melanosomal RAB38 or TYRP1, but not if T cells targeted oncogenic CDK4^{R24C}.

As reported previously, inflammation-induced melanoma dedifferentiation can be reversible, at least in some cases (Landsberg et al., 2012; Riesenberg et al., 2015). In agreement, we found examples of moderate to complete re-expression of RAB38-NFhgp100 or TYRP1-NFhgp100 in recurrent melanomas upon culturing *ex vivo* under non-inflammatory conditions (Figure 5G). During ACT, activated T cells and macrophages are important sources of IFN-γ and TNF-α, among other cytokines (Glodde et al., 2017; Landsberg et al., 2012). To mimic an inflamed microenvironment *in vitro*, we exposed all three melanoma models to conditioned medium from activated T cells (T-cell-conditioned medium, TCM), which confirmed decreased expression of melanosomal TYRP1-NFhgp100 and RAB38-NFhgp100, but not CDK4^{R24C}-NFhgp100 (Figure 5H). Pro-apoptotic effects by TCM were blocked by IFN-γ depletion (Figures S5A and S5B). Combined exposure to IFN-γ and TNF-α was particularly effective in downregulating the expression of TYRP1-NFhgp100 and RAB38-NFhgp100, while CDK4^{R24C}-NFhgp100 remained unchanged (Figure 5I). Altogether, the data showed that inflammation-induced dedifferentiation provided a specific benefit for immune escape if T cells targeted melanosomal antigens, but not if T cells were directed against oncogenic CDK4^{R24C}.

Antigen Loss and Melanoma Dedifferentiation Determine Immune Phenotypes

Next, we were interested in the immune phenotypes of recurrent melanomas. GSEA revealed that interferon response signatures were enriched in both RAB38-NFhgp100- and CDK4^{R24C}-NFhgp100-recurrent melanomas (Figures 6A and 6B). This was also true for TYRP1-NFhgp100-recurrent melanomas with decreased but not lost antigen expression (R5-7), in contrast to the cases with hardwired antigen loss (R1–4, R8) (Figure S6A). When directly comparing all groups, recurrent melanomas with a positive target antigen status were interferon high, whereas those with genomic hardwired antigen loss were interferon low (Figures 6C and S6B).

An interferon-high phenotype is usually associated with T cell infiltration (Bald et al., 2014b; Gajewski et al., 2017). Consistently, RAB38-NFhgp100- and CDK4^{R24C}-NFhgp100-recurrent melanomas showed increased T cell transcript level (e.g., *Cd8a*) suggestive of pmel-1 T cell persistence (Figures 6D and 6H). Flow cytometry specified that on average, 37% (±28% SD) or 47% (±33% SD) of infiltrating CD8$^+$ T cells in recurrent RAB38-NFhgp100 or CDK24^{R24C}-NFhgp100 melanomas, respectively, were actually pmel-1 T cells, though frequencies were quite variable (data not shown). Noteworthy, we found that myeloid cell transcripts, a surrogate for myeloid cell content, were increased in RAB38-NFhgp100- but not in CDK4^{R24C}-NFhgp100-recurrent melanomas (Figures 6E and 6I). In view of the dedifferentiated phenotype of RAB38-NFhgp100-recurrent melanomas, this result was in line with our previous work showing that dedifferentiated melanoma cells abundantly released chemokines involved in myeloid cell recruitment (Riesenberg et al., 2015). Supportively, myeloid cell recruiting chemokine genes were also induced in RAB38-NFhgp100-recurrent melanomas (Figures 6F). Altogether, our esACT approach enabled us to demonstrate that melanoma dedifferentiation and increased myeloid cell content were specific features of immune escape if T cells targeted melanosomal RAB38-NFhgp100, but not CDK4^{R24C}-NFhgp100. Previously, we showed that the intratumor injections of CpG and Poly(I:C) as part of the ACT protocol induced strong myeloid cell recruitment early during treatment (Glodde et al., 2017), which is why we wondered whether this was also true in CDK4^{R24C}-NFhgp100 melanomas. Additional transcriptome analyses revealed a prominent peak of T cell and myeloid cell transcripts, as well as pro-inflammatory cytokines, shortly after completion of the esACT protocol (Figures S6C–S6E and S6G–S6I). Thus, different from the persistently elevated T cell content in CDK4^{R24C}-NFhgp100-recurrent melanomas (Figures S6C and S6G), myeloid cell content returned to "baseline" level of non-treated controls (Figures S6D and S6H), which was in contrast to the myeloid-rich RAB38-NFhgp100-recurrent melanomas (Figure 6E). The same was true for most cytokines and chemokines, with notable exceptions such as IFN-γ and Cxcl9 linked to T cell activation and recruitment (Figures S6E and S6I). The pronounced pro-inflammatory microenvironment early during treatment also resulted in transient dedifferentiation of CDK4^{R24C}-NFhgp100 melanomas (Figures S6F and S6J), which was expected as inflammation was a well-established inducer of melanoma phenotype switching. Given that the differentiation status of recurrent melanomas returned to baseline of non-treated controls, it further confirmed that dedifferentiation did not promote immune escape of CDK4^{R24C}-NFhgp100 melanomas.

This prompted us to search for additional immune escape mechanisms in CDK4^{R24C}-NFhgp100-recurrent melanomas, as CDK4^{R24C} antigen persistence, contrary to RAB38, should allow for salvage therapy by T cell reinvigoration. Interferon-high and T-cell-rich microenvironments usually correlate

(E) GSEA plots for Verfaillie invasive signature comparing recurrent (R5-7) HC.*Pmel*$^{-/-}$.TYRP1-NFhgp100 and recurrent (R) HC.*Pmel*$^{-/-}$.CDK4^{R24C}-NFhgp100 melanomas. FDR: false discovery rate, ES: enrichment score.

(F) *Axl* mRNA expression by RNA-seq (log2) in indicated non-treated (NT) and esACT-recurrent (R) HC.*Pmel*$^{-/-}$ melanomas. Statistics: ***FDR < 0.001, *FDR < 0.05, unpaired two-sided t test.

(G) Representative histograms showing mNeon expression by flow cytometry of indicated HC.*Pmel*$^{-/-}$.RAB38-NFhgp100- (left) or HC.*Pmel*$^{-/-}$.TYRP1-NFhgp100- (right) recurrent melanomas on day 0 and day 19 or day 14 of *ex vivo* culture.

(H) Relative mNeon expression (MFI: mean fluorescence intensity) measured by flow cytometry of indicated HC.*Pmel*$^{-/-}$ melanoma cells treated with T-cell-conditioned medium (TCM) for 5 days (n = 3, mean ± SD).

(I) Relative mNeon expression (MFI: mean fluorescence intensity) measured by flow cytometry of indicated HC.*Pmel*$^{-/-}$ melanoma cells treated with IFN-γ (500 U ml^{-1}) and/or TNF-α (500U ml^{-1}) for 5 days (n = 3, mean ± SD). Statistics: ****p < 0.0001, ***p < 0.001, **p < 0.01, *p < 0.05, n.s.: not significant; unpaired two-sided t test.

See also Figure S5.

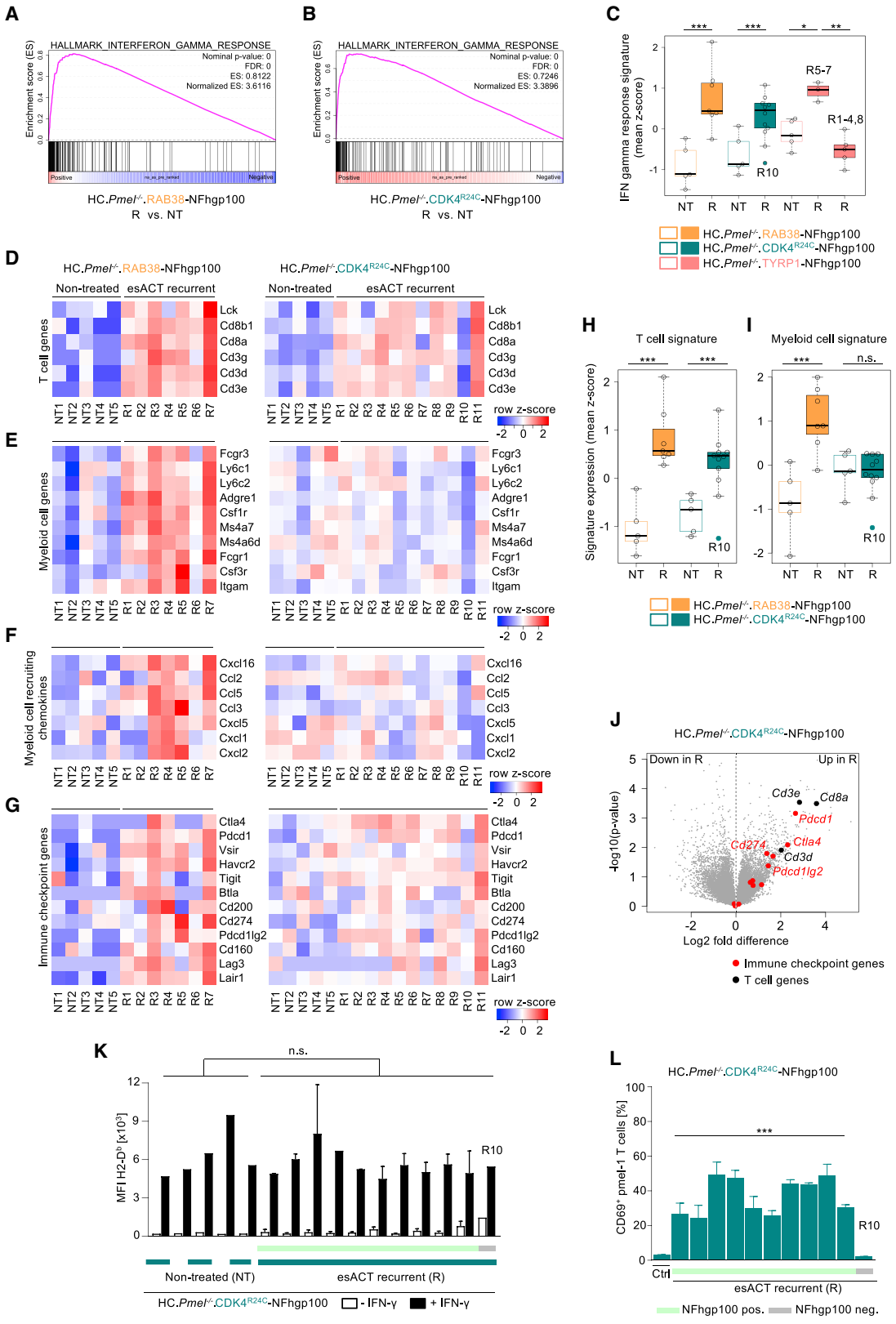

Figure 6. Immune Landscape of esACT-Recurrent Melanomas Determined by Target Antigen Status and Adaptive Dedifferentiation

(A and B) GSEA plots for interferon gamma response signature comparing non-treated (NT) and recurrent (R) HC.*Pmel*$^{-/-}$.RAB38-NFhgp100 (A) and HC.*Pmel*$^{-/-}$.CDK4^{R24C}-NFhgp100 (B) melanomas. FDR: false discovery rate, ES: enrichment score.

(legend continued on next page)

with good responses to immune checkpoint inhibitors (Bald et al., 2014b; Cristescu et al., 2018; Gajewski et al., 2017). Chronic interferon signaling was previously linked to a multigenic resistance program, which included T cell inhibitory ligands such as PD-L1 (Benci et al., 2016). In line, we found increased transcript level of T cell inhibitory ligands and receptors in recurrent melanomas, though the picture was heterogeneous (Figure 6G). *Pdcd1* (PD-1), *Cd274* (PD-L1), and *Ctla4* were the most significantly induced immune checkpoint genes analyzed (Figure 6J). This suggested that interferon-driven feedback inhibition by the PD-1:PD-L1 axis could contribute to immune escape of CDK4^{R24C}-NFhgp100 melanomas, which was a tractable target for salvage therapy with immune checkpoint inhibitors. Prior to this, we excluded acquired defects in antigen presentation as predominant resistance mechanism in CDK4^{R24C}-NFhgp100-recurrent melanomas. Isolated melanoma cells showed normal induction of MHC class I surface expression and recognition by pmel-1 T cells apart from the case (R10) with hardwired antigen loss (Figures 6K and 6L).

Responsiveness of Recurrent Melanomas to Anti-PD-L1 Salvage Therapy

For salvage immune checkpoint inhibition (sICI) with anti-PD-L1, CDK4^{R24C}-NFhgp100 melanoma-bearing mice (n = 21) were first treated with esACT. Recurrent melanomas (n = 13) were then treated with anti-PD-L1 antibody (sICI-1–sICI-13) at the time when tumors resumed growth (Figure 7A). Responses to sICI could be broadly subdivided into three groups. First, in cases with moderate responses to esACT (n = 5), sICI was ineffective (e.g., sICI-7) (Figure 7B), and antigen loss did not occur based on mNeon (CDK4^{R24C}-NFhgp100) expression in melanoma cells (Figure 7C). Second, in cases with good responses to esACT (n = 5), we observed partial regressions (e.g., sICI-3, -10) or stable disease (e.g., sICI-9) upon sICI until tumor growth resumed (Figure 7D). These sICI-recurrent melanomas were antigen positive, though we also noted an mNeon negative subpopulation (60.2%) in sICI-3 (Figure 7E). Third, in cases with complete regression to esACT (n = 3), we found that all recurrent melanomas (e.g., sICI-4 and sICI-5) were unresponsive to sICI (Figure 7D). Outgrowth of antigen loss variants was a reasonable explanation and confirmed by mNeon negativity for two cases (e.g., sICI-4) (Figure 7E).

Unexpectedly, melanoma cells isolated from sICI-5 showed normal antigen expression (Figure 7E), and sequencing excluded truncating mutations (data not shown). *In vitro*, pmel-1 T cells failed to recognize sICI-5 cells similar to antigen-negative sICI-4 or HC.*Pmel*$^{-/-}$ cells (Figure 7F). We therefore analyzed MHC class I surface expression of sICI-5 cells and found that H2-D^{b}, which is responsible for hgp100 epitope presentation, was poorly induced by IFN-γ (Figures 7G and 7H). Of note, the beta-2-microglobulin gene, a common genetic cause of defective antigen presentation, was not mutated in sICI-5 cells (data not shown). Thus, reduced MHC class I expression and antigen presentation provided an explanation for the lack of recognition of sICI-5 cells by pmel-1 T cells *in vitro* and immune escape *in vivo*. We also evaluated PD-L1 blockade concomitant with esACT as alternative strategy against CDK4^{R24C}-NFhgp100 melanomas showing better efficacy when compared to esACT plus IgG controls (Figure S7). In summary, our esACT approach and sICI of recurrent melanomas identified different genetic and non-genetic mechanisms of immune escape (Figure S7G).

DISCUSSION

Personalized cancer immunotherapy is rapidly developing, and clinical trials are evaluating antigen-specific T cell therapies such as ACT or vaccines (Chandran et al., 2015; Chodon et al., 2014; Nowicki et al., 2019; Ott et al., 2017; Sahin et al., 2017; Schumacher et al., 2014). A key challenge is the selection of the right target epitope(s), which can be derived from mutated or non-mutated tumor antigens (Blankenstein et al., 2015; Hinrichs and Restifo, 2013). Peptide-MHC binding affinity is an important determinant (Engels et al., 2013), and fortunately computational algorithms for *in silico* prediction have substantially improved (Bulik-Sullivan et al., 2018; Jurtz et al., 2017; O'Donnell et al., 2018). Additional epitope qualities seem to correlate with potent long-term anti-tumor responses (Balachandran et al., 2017). Aside from these epitope features, our knowledge is limited, in particular, how regulation and function of the epitope-producing genes influence immune escape from personalized T cell therapy.

We therefore devised CRISPitope, an approach to generate syngeneic mouse melanomas expressing the same (standardized) epitope fused to different endogenous gene products. As a proof of concept for "epitope-standardized" ACT, we directed the same effector CD8^{+} T cells against TYRP1 or RAB38, two typical MDAs, or CDK4^{R24C}, an oncogenic driver, that altogether represented two major types of melanoma antigens with different regulation and cellular functions (Walton et al., 2006; Wang et al., 1995; Wölfel et al., 1995). Previous experimental studies have also investigated ACT targeting different gene products, but comparability is limited due to different epitopes

(C) All group comparison of interferon gamma response gene expression. NT: non-treated; R: esACT-recurrent melanoma. Statistics: ***FDR < 0.001, **FDR < 0.01, *FDR < 0.05, unpaired two-sided t test.
(D–G) Heatmap of T cell gene (D), myeloid cell gene (E), myeloid cell-recruiting chemokines (F), and immune checkpoint gene (G) expression in indicated non-treated (NT) and recurrent (R) melanomas.
(H and I) Quantified T cell (H) and myeloid cell (I) signature expression from (D) and (E). Statistics: ***FDR < 0.001, n.s.: not significant, unpaired two-sided t test.
(J) Volcano plot for differentially expressed genes between non-treated (NT) and recurrent (R) HC.*Pmel*$^{-/-}$.CDK4^{R24C}-NFhgp100 melanomas. Highlighted: immune checkpoint genes (red) and T cell genes (black).
(K) H2-D^{b} surface expression (MFI: mean fluorescence intensity) measured by flow cytometry on non-treated and recurrent HC.*Pmel*$^{-/-}$.CDK4^{R24C}-NFhgp100 melanoma cells exposed to IFN-γ (1000 U ml^{-1}) for 72 h (n ≥ 1; mean ± SD). Statistics: n.s.: not significant; Mann-Whitney-test.
(L) Flow cytometric quantification of CD69 surface expression on CD8^{+} CD90.1^{+} pmel-1 T cells co-cultured (16 h) with IFN-γ pre-treated (72 h) melanoma cells from indicated recurrent melanomas (n = 3; mean ± SD). Statistics: ***p < 0.001; unpaired two-sided t test.
See also Figure S6.

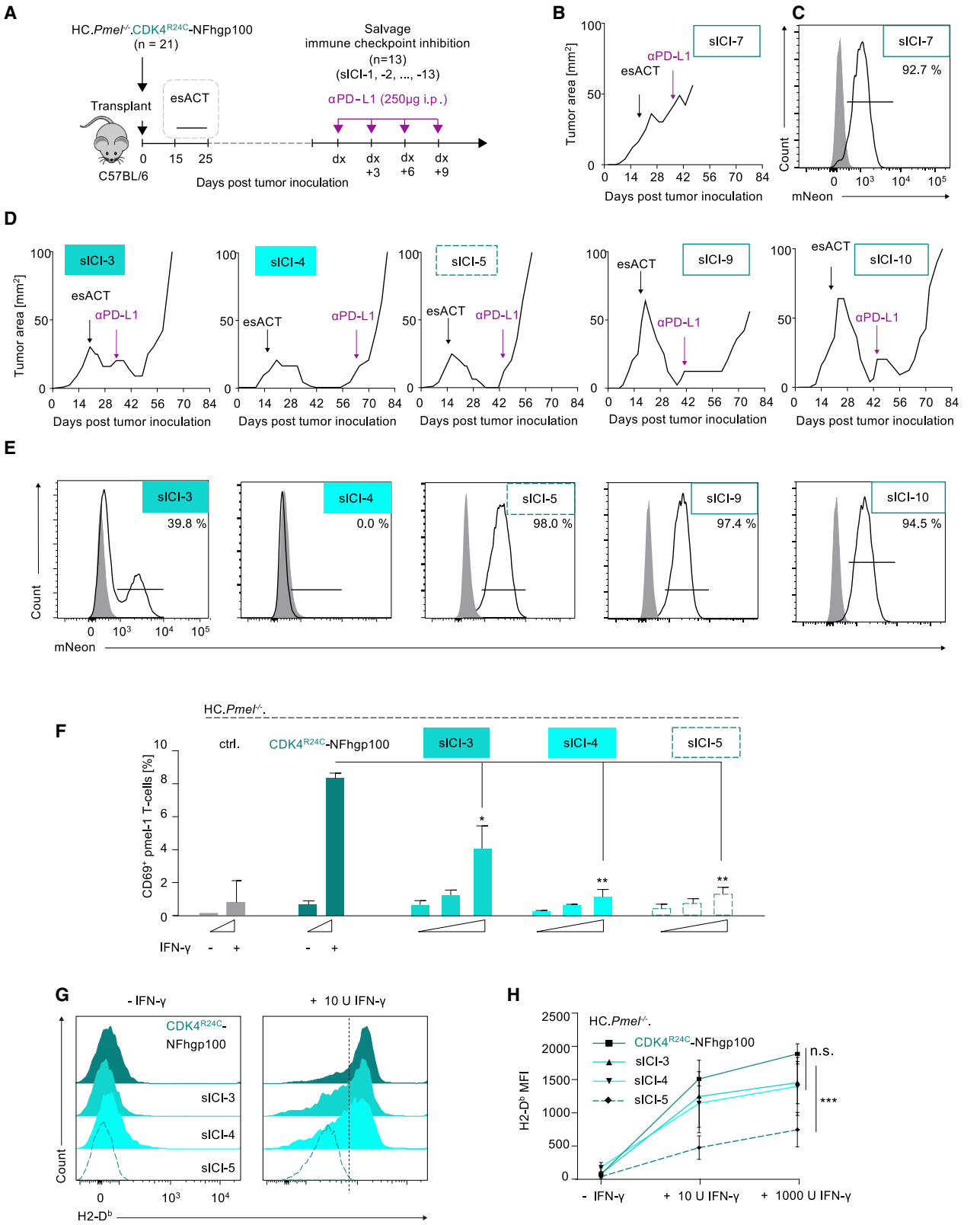

Figure 7. Salvage Therapy for esACT-Recurrent Melanomas with Anti-PD-L1 Immune Checkpoint Inhibitor

(A) Experimental setup of esACT and salvage ICI therapy (sICI) with αPD-L1 of C57BL/6 mice bearing HC.*Pmel*$^{-/-}$.CDK4^{R24C}-NFhgp100 melanomas. Numbers as indicated.

(legend continued on next page)

or ectopic antigen expression lacking endogenous regulation patterns (Anders et al., 2011; Leisegang et al., 2016; Overwijk et al., 1998).

By the strength of our approach, we were able to demonstrate that inflammation-induced melanoma dedifferentiation was not a general immune escape mechanism, as it was only evident when T cells targeted melanosomal proteins, but not CDK4^{R24C}. We propose that our findings are also relevant to spontaneous melanoma immune surveillance. Melanoma patients frequently have endogenous T cell responses against MDAs (Brichard et al., 1993; Kawakami et al., 1994; Wang et al., 1995), but surprisingly little is known about the phenotypic co-evolution of their melanomas. The same is true for MDA-directed T cell responses in the context of immune checkpoint inhibition. As melanoma dedifferentiation reduces sensitivity to MAPK inhibitors (Konieczkowski et al., 2014; Müller et al., 2014), we speculate that MDA-directed T cell responses driving phenotypic co-evolution have a more profound impact on melanoma therapy than currently anticipated.

Furthermore, our approach identified various genetic and epigenetic mechanisms of antigen loss or presentation defects causing immune evasion (Rodig et al., 2018; Zhao et al., 2016). Selective transcriptional silencing of the immunogenic (epitope-tagged) allele in one case (TYRP1-NFhgp100 R2) emphasized the importance of epigenetic regulation for complex antigen dynamics as seen in longitudinal samples from ACT-treated melanoma patients (Verdegaal et al., 2016). One scenario is that T cell responses enforce clonal outgrowth of tumor cells with randomly silenced antigen expression, even in an allele-specific manner. Interestingly, a substantial part of the transcriptome in single cells has been recently found to be subject to dynamic monoallelic expression (Reinius et al., 2016), which warrants future work with regard to antigen dynamics in tumors under immunotherapy.

Our data also showed that immune phenotypes of ACT-recurrent melanomas were determined by the underlying resistance mechanisms. First, recurrent melanomas with hardwired complete antigen loss exhibited a "cold" (IFN-γ-low, T-cell-poor) tumor microenvironment (TME). A likely explanation is that lack of antigen expression and T cell recognition also restrained the recruitment and activation of other immune cells within the TME. Consistent with current concepts of the cold TME (Ayers et al., 2017; Cristescu et al., 2018; Gajewski et al., 2017), relapsed melanomas with antigen loss or defective antigen presentation were unresponsive to salvage ICI. Along these lines, human melanomas acquiring resistance to ICI by *B2M* loss (Zaretsky et al., 2016; Zhao et al., 2016), which abrogates antigen presentation and immune recognition, are reported to be poorly infiltrated by T cells (Sade-Feldman et al., 2017).

Second, recurrent melanomas without hardwired antigen loss showed a "hot" (IFN-γ-high, T-cell-rich) TME. Here, we suppose that continuous antigen expression and T cell recognition sustain an inflamed TME. In line with the proposed interferon-driven resistance program involving PD-L1 induction, among others (Ayers et al., 2017; Benci et al., 2016; Cristescu et al., 2018), the hot TME of ACT-recurrent CDK4^{R24C}-hgp100 melanomas allowed for effective ICI salvage therapy, at least in some cases. Of note, other IFN-γ driven mechanisms contribute to immunotherapy resistance such as genomic instability of tumor cells, myeloid cell rewiring, and higher susceptibility of T cells to apoptosis (Glodde et al., 2017; Jacquelot et al., 2019; Pai et al., 2019; Takeda et al., 2017), which argues for additional and complementary salvage treatment strategies.

Third, we showed that enforced dedifferentiation driven by a T cell response against melanosomal RAB38 favored myeloid cell persistence in recurrent melanomas, which was not the case if T cells targeted CDK4^{R24C}. This demonstrated that phenotype and immune cell composition of ACT-recurrent melanomas were directly dependent on the target antigen due to different immune selection pressures. We propose that such interrelationships between tumor cell phenotypes and immune cell composition also exist in other cancer entities, particularly when targeting lineage antigens.

In summary, we established a versatile and powerful experimental approach to study the diversity and context dependency of immune escape from T cell therapy. It can be easily adapted to different syngeneic mouse tumor models, which makes it an attractive methodology to many other laboratories. We also believe that our approach will help to improve the design of personalized cancer immunotherapy.

Limitations

Our study also has limitations with regard to generality and clinical relevance. In the future, it will be important to assay a larger number of endogenous targets, particularly additional oncogenic and other essential gene products. Multiplexing of different targets combined with single-cell analyses could be a strategy to increase the throughput of our CRISPitope approach, at least for the assessment of melanoma cell-intrinsic immune escape mechanisms. Further, our work is experimental and its relevance to human melanoma remains to be confirmed. A prediction from our study is that MDA-directed T cell responses are central drives of melanoma dedifferentiation in the course of the disease. Prospective clinical studies will be needed that

(B) Individual tumor growth curve of sICI-7.
(C) Histogram showing mNeon expression by flow cytometry in melanoma cells isolated from sICI-7 compared to mNeon-negative control cells (gray).
(D and E) Individual tumor growth curves of exemplary cases (D) and corresponding histograms (E) showing mNeon expression by flow cytometry compared to mNeon-negative control cells (gray).
(F) Quantification of CD69 surface expression on CD8$^+$ CD90.1$^+$ pmel-1 T cells co-cultured (16 h) with indicated melanoma cells pre-treated with increasing concentrations of IFN-γ (0, 10 or 1000 U ml^{-1}) for 72 h. (n = 3; mean ± SD). Statistics: ***p < 0.001, *p < 0.05; n.s.: not significant; unpaired two-sided t test.
(G) Representative histograms showing induction of H2-D^b surface expression by flow cytometry on indicated melanoma cells treated with IFN-γ (10 U ml^{-1}) for 72 h. Controls were left untreated.
(H) Quantification of H2-D^b surface expression (MFI: mean fluorescence intensity) on indicated melanoma cells treated with increasing concentrations of IFN-γ for 72 h (n = 3; mean ± SD). ***p < 0.001, n.s.: not significant; Mann-Whitney-test.
See also Figure S7.

longitudinally sample melanoma tissues for phenotype assessment and simultaneously monitor MDA-directed T cell responses.

STAR★METHODS

Detailed methods are provided in the online version of this paper and include the following:

- KEY RESOURCES TABLE
- RESOURCE AVAILABILITY
  - Lead contact
  - Materials availability
  - Data and code availability
- EXPERIMENTAL MODEL AND SUBJECT DETAILS
  - Mice
  - Cell lines
  - Primary cell cultures
- METHOD DETAILS
  - Generation of CRISPitope plasmids
  - Generation of HC.*Pmel*$^{-/-}$ cell line
  - Generation of CRISPitope-engineered cell lines
  - Western blotting
  - Epifluorescence microscopy
  - *In vitro* pmel-1 T cell activation assay
  - *In vitro* gBT-I T cell activation assay
  - Tumor transplantation experiments
  - Adoptive cell transfer (ACT) immunotherapy
  - Salvage immune checkpoint inhibition therapy
  - Concomitant ACT and checkpoint immunotherapy
  - Tissue digestion and processing
  - Flow cytometry
  - PCR analysis of recurrent melanomas
  - Melanoma cell dedifferentiation assay
  - Apoptosis assay
  - 3′mRNA-Seq analysis of melanomas
  - Gene set enrichment analysis
- QUANTIFICATION AND STATISTICAL ANALYSIS
  - Statistical analyses
  - Selection of statistical tests

SUPPLEMENTAL INFORMATION

Supplemental Information can be found online at https://doi.org/10.1016/j.immuni.2020.07.007.

ACKNOWLEDGMENTS

We thank P. Wurst and An. Dolf for help with flow cytometry. We thank the UKB core facilities (flow cytometry and NGS). This work was supported by an NHMRC Early Career fellowship (grant number 1124690) and an EMBO Long Term Fellowship ALTF (grant number 945-2015) to T.B., the Deutsche Krebshilfe (German Cancer Aid) through a junior research group grant within the Mildred Scheel School of Oncology (MSSO) Cologne-Bonn (70113307) to N.G., a scholarship within the "Mildred Scheel Stiftung für Krebsforschung" to M.B., the Deutsche Forschungsgemeinschaft (DFG, German Research Foundation) within GRK 2168 to M.H., scholarships by the University of Melbourne to M.E. and E.B., a scholarship to M.E. within GRK 2168, and the DFG under Germany's Excellence Strategy–EXC2151–390873048. M.J.S. was supported by NHMRC Investigator (1173958) and Program (1132519) grants. T.G. and M.H. are supervisors in the GRK 2168 international graduate school, Bonn-Melbourne. M.H. is a member of the DFG Excellence Cluster ImmunoSensation^2 (EXC 2151).

AUTHOR CONTRIBUTIONS

Conceptualization, M.E., N.G., T.G., T.T., and M.H.; Methodology, M.E., N.G., D.v.d.B.-K.., and M.D.; Software, M.H.; Validation, M.E., N.G., J.L., E.B., D.H., T.B., and M.Y.; Formal Analysis, M.E. and N.G.; Investigation, M.E., N.G., E.B., D.H., J.L., P.A., T.B., D.v.d.B.-K., M.B., H.N.B., M.D., and M.Y.; Resources, J.L., M.J.S., T.G., T.T., and M.H.; Data Curation, M.E., N.G., T.B., T.G., and M.H.; Writing – Original Draft, M.E., N.G., and M.H.; Writing – Review & Editing, M.E., T.G., E.B., N.G., L.F., and M.H.; Supervision, N.G., T.G., and M.H.; Project Administration, T.G. and M.H.; Funding Acquisition, T.B., N.G., T.G., and M.H.

DECLARATION OF INTERESTS

T.B. has research agreements with Bristol-Myers Squibb and Ena Therapeutics and is on the scientific advisory board for Oncomyx, none of which deals with the submitted work. M.J.S. has scientific research agreements with Bristol-Myers Squibb and Tizona Therapeutics and is an advisory board member for Compass Therapeutics and Tizona Therapeutics, all outside the submitted work. T.T. and M.H. declare receipt of honoraria for the scientific advisory board of Novartis unrelated to the submitted work. M.H. declares receipt of honoraria from Bristol-Myers Squibb unrelated to this work.

Received: March 5, 2019
Revised: April 5, 2020
Accepted: July 8, 2020
Published: August 3, 2020

REFERENCES

Anders, K., Buschow, C., Herrmann, A., Milojkovic, A., Loddenkemper, C., Kammertoens, T., Daniel, P., Yu, H., Charo, J., and Blankenstein, T. (2011). Oncogene-targeting T cells reject large tumors while oncogene inactivation selects escape variants in mouse models of cancer. Cancer Cell *20*, 755–767.

Ayers, M., Lunceford, J., Nebozhyn, M., Murphy, E., Loboda, A., Kaufman, D.R., Albright, A., Cheng, J.D., Kang, S.P., Shankaran, V., et al. (2017). IFN-γ-related mRNA profile predicts clinical response to PD-1 blockade. J. Clin. Invest. *127*, 2930–2940.

Balachandran, V.P., Łuksza, M., Zhao, J.N., Makarov, V., Moral, J.A., Remark, R., Herbst, B., Askan, G., Bhanot, U., Senbabaoglu, Y., et al.; Australian Pancreatic Cancer Genome Initiative; Garvan Institute of Medical Research; Prince of Wales Hospital; Royal North Shore Hospital; University of Glasgow; St Vincent's Hospital; QIMR Berghofer Medical Research Institute; University of Melbourne, Centre for Cancer Research; University of Queensland, Institute for Molecular Bioscience; Bankstown Hospital; Liverpool Hospital; Royal Prince Alfred Hospital, Chris O'Brien Lifehouse; Westmead Hospital; Fremantle Hospital; St John of God Healthcare; Royal Adelaide Hospital; Flinders Medical Centre; Envoi Pathology; Princess Alexandria Hospital; Austin Hospital; Johns Hopkins Medical Institutes; ARC-Net Centre for Applied Research on Cancer (2017). Identification of unique neoantigen qualities in long-term survivors of pancreatic cancer. Nature *551*, 512–516.

Bald, T., Quast, T., Landsberg, J., Rogava, M., Glodde, N., Lopez-Ramos, D., Kohlmeyer, J., Riesenberg, S., van den Boorn-Konijnenberg, D., Hömig-Hölzel, C., et al. (2014a). Ultraviolet-radiation-induced inflammation promotes angiotropism and metastasis in melanoma. Nature *507*, 109–113.

Bald, T., Landsberg, J., Lopez-Ramos, D., Renn, M., Glodde, N., Jansen, P., Gaffal, E., Steitz, J., Tolba, R., Kalinke, U., et al. (2014b). Immune cell-poor melanomas benefit from PD-1 blockade after targeted type I IFN activation. Cancer Discov. *4*, 674–687.

Bassani-Sternberg, M., Bräunlein, E., Klar, R., Engleitner, T., Sinitcyn, P., Audehm, S., Straub, M., Weber, J., Slotta-Huspenina, J., Specht, K., et al. (2016). Direct identification of clinically relevant neoepitopes presented on

native human melanoma tissue by mass spectrometry. Nat. Commun. *7*, 13404.

Benci, J.L., Xu, B., Qiu, Y., Wu, T.J., Dada, H., Twyman-Saint Victor, C., Cucolo, L., Lee, D.S.M., Pauken, K.E., Huang, A.C., et al. (2016). Tumor Interferon Signaling Regulates a Multigenic Resistance Program to Immune Checkpoint Blockade. Cell *167*, 1540–1554.e12.

Blankenstein, T., Leisegang, M., Uckert, W., and Schreiber, H. (2015). Targeting cancer-specific mutations by T cell receptor gene therapy. Curr. Opin. Immunol. *33*, 112–119.

Brichard, V., Van Pel, A., Wölfel, T., Wölfel, C., De Plaen, E., Lethé, B., Coulie, P., and Boon, T. (1993). The tyrosinase gene codes for an antigen recognized by autologous cytolytic T lymphocytes on HLA-A2 melanomas. J. Exp. Med. *178*, 489–495.

Bulik-Sullivan, B., Busby, J., Palmer, C.D., Davis, M.J., Murphy, T., Clark, A., Busby, M., Duke, F., Yang, A., Young, L., et al. (2018). Deep learning using tumor HLA peptide mass spectrometry datasets improves neoantigen identification. Nat. Biotechnol. *37*, 55–63.

Chandran, S.S., Paria, B.C., Srivastava, A.K., Rothermel, L.D., Stephens, D.J., Dudley, M.E., Somerville, R., Wunderlich, J.R., Sherry, R.M., Yang, J.C., et al. (2015). Persistence of CTL clones targeting melanocyte differentiation antigens was insufficient to mediate significant melanoma regression in humans. Clin. Cancer Res. *21*, 534–543.

Chodon, T., Comin-Anduix, B., Chmielowski, B., Koya, R.C., Wu, Z., Auerbach, M., Ng, C., Avramis, E., Seja, E., Villanueva, A., et al. (2014). Adoptive transfer of MART-1 T-cell receptor transgenic lymphocytes and dendritic cell vaccination in patients with metastatic melanoma. Clin. Cancer Res. *20*, 2457–2465.

Cristescu, R., Mogg, R., Ayers, M., Albright, A., Murphy, E., Yearley, J., Sher, X., Liu, X.Q., Lu, H., Nebozhyn, M., et al. (2018). Pan-tumor genomic biomarkers for PD-1 checkpoint blockade-based immunotherapy. Science *362*, https://doi.org/10.1126/science.aar3593.

Engels, B., Engelhard, V.H., Sidney, J., Sette, A., Binder, D.C., Liu, R.B., Kranz, D.M., Meredith, S.C., Rowley, D.A., and Schreiber, H. (2013). Relapse or eradication of cancer is predicted by peptide-major histocompatibility complex affinity. Cancer Cell *23*, 516–526.

Gajewski, T.F., Corrales, L., Williams, J., Horton, B., Sivan, A., and Spranger, S. (2017). Cancer Immunotherapy Targets Based on Understanding the T Cell-Inflamed Versus Non-T Cell-Inflamed Tumor Microenvironment. Adv. Exp. Med. Biol. *1036*, 19–31.

Glodde, N., Bald, T., van den Boorn-Konijnenberg, D., Nakamura, K., O'Donnell, J.S., Szczepanski, S., Brandes, M., Eickhoff, S., Das, I., Shridhar, N., et al. (2017). Reactive Neutrophil Responses Dependent on the Receptor Tyrosine Kinase c-MET Limit Cancer Immunotherapy. Immunity *47*, 789–802.e9.

Goding, C.R., and Arnheiter, H. (2019). MITF-the first 25 years. Genes Dev. *33*, 983–1007.

Hanada, K.-I., Yu, Z., Chappell, G.R., Park, A.S., and Restifo, N.P. (2019). An effective mouse model for adoptive cancer immunotherapy targeting neoantigens. JCI Insight *4*, e124405.

Hinrichs, C.S., and Restifo, N.P. (2013). Reassessing target antigens for adoptive T-cell therapy. Nat. Biotechnol. *31*, 999–1008.

Hoek, K.S., Eichhoff, O.M., Schlegel, N.C., Döbbeling, U., Kobert, N., Schaerer, L., Hemmi, S., and Dummer, R. (2008). In vivo switching of human melanoma cells between proliferative and invasive states. Cancer Res. *68*, 650–656.

Jacquelot, N., Yamazaki, T., Roberti, M.P., Duong, C.P.M., Andrews, M.C., Verlingue, L., Ferrere, G., Becharef, S., Vétizou, M., Daillère, R., et al. (2019). Sustained Type I interferon signaling as a mechanism of resistance to PD-1 blockade. Cell Res. *29*, 846–861.

Jurtz, V., Paul, S., Andreatta, M., Marcatili, P., Peters, B., and Nielsen, M. (2017). NetMHCpan-4.0: Improved Peptide-MHC Class I Interaction Predictions Integrating Eluted Ligand and Peptide Binding Affinity Data. J. Immunol. *199*, 3360–3368.

Kawakami, Y., Eliyahu, S., Delgado, C.H., Robbins, P.F., Sakaguchi, K., Appella, E., Yannelli, J.R., Adema, G.J., Miki, T., and Rosenberg, S.A. (1994). Identification of a human melanoma antigen recognized by tumor-infiltrating lymphocytes associated with in vivo tumor rejection. Proc. Natl. Acad. Sci. USA *91*, 6458–6462.

Konieczkowski, D.J., Johannessen, C.M., Abudayyeh, O., Kim, J.W., Cooper, Z.A., Piris, A., Frederick, D.T., Barzily-Rokni, M., Straussman, R., Haq, R., et al. (2014). A melanoma cell state distinction influences sensitivity to MAPK pathway inhibitors. Cancer Discov. *4*, 816–827.

Landsberg, J., Kohlmeyer, J., Renn, M., Bald, T., Rogava, M., Cron, M., Fatho, M., Lennerz, V., Wölfel, T., Hölzel, M., and Tüting, T. (2012). Melanomas resist T-cell therapy through inflammation-induced reversible dedifferentiation. Nature *490*, 412–416.

Law, C.W., Chen, Y., Shi, W., and Smyth, G.K. (2014). voom: Precision weights unlock linear model analysis tools for RNA-seq read counts. Genome Biol. *15*, R29.

Leisegang, M., Engels, B., Schreiber, K., Yew, P.Y., Kiyotani, K., Idel, C., Arina, A., Duraiswamy, J., Weichselbaum, R.R., Uckert, W., et al. (2016). Eradication of Large Solid Tumors by Gene Therapy with a T-Cell Receptor Targeting a Single Cancer-Specific Point Mutation. Clin. Cancer Res. *22*, 2734–2743.

Liao, Y., Smyth, G.K., and Shi, W. (2013). The Subread aligner: fast, accurate and scalable read mapping by seed-and-vote. Nucleic Acids Res. *41*, e108.

Liberzon, A., Birger, C., Thorvaldsdóttir, H., Ghandi, M., Mesirov, J.P., and Tamayo, P. (2015). The Molecular Signatures Database (MSigDB) hallmark gene set collection. Cell Syst. *1*, 417–425.

Łuksza, M., Riaz, N., Makarov, V., Balachandran, V.P., Hellmann, M.D., Solovyov, A., Rizvi, N.A., Merghoub, T., Levine, A.J., Chan, T.A., et al. (2017). A neoantigen fitness model predicts tumour response to checkpoint blockade immunotherapy. Nature *551*, 517–520.

Macleod, B.L., Bedoui, S., Hor, J.L., Mueller, S.N., Russell, T.A., Hollett, N.A., Heath, W.R., Tscharke, D.C., Brooks, A.G., and Gebhardt, T. (2014). Distinct APC subtypes drive spatially segregated CD4+ and CD8+ T-cell effector activity during skin infection with HSV-1. PLoS Pathog. *10*, e1004303.

Mehta, A., Kim, Y.J., Robert, L., Tsoi, J., Comin-Anduix, B., Berent-Maoz, B., Cochran, A.J., Economou, J.S., Tumeh, P.C., Puig-Saus, C., and Ribas, A. (2018). Immunotherapy Resistance by Inflammation-Induced Dedifferentiation. Cancer Discov. *8*, 935–943.

Müller, J., Krijgsman, O., Tsoi, J., Robert, L., Hugo, W., Song, C., Kong, X., Possik, P.A., Cornelissen-Steijger, P.D.M., Geukes Foppen, M.H., et al. (2014). Low MITF/AXL ratio predicts early resistance to multiple targeted drugs in melanoma. Nat. Commun. *5*, 5712.

Nowicki, T.S., Berent-Maoz, B., Cheung-Lau, G., Huang, R.R., Wang, X., Tsoi, J., Kaplan-Lefko, P., Cabrera, P., Tran, J., Pang, J., et al. (2019). A Pilot Trial of the Combination of Transgenic NY-ESO-1-reactive Adoptive Cellular Therapy with Dendritic Cell Vaccination with or without Ipilimumab. Clin. Cancer Res. *25*, 2096–2108.

O'Donnell, T.J., Rubinsteyn, A., Bonsack, M., Riemer, A.B., Laserson, U., and Hammerbacher, J. (2018). MHCflurry: Open-Source Class I MHC Binding Affinity Prediction. Cell Syst. *7*, 129–132.e4.

Ott, P.A., Hu, Z., Keskin, D.B., Shukla, S.A., Sun, J., Bozym, D.J., Zhang, W., Luoma, A., Giobbie-Hurder, A., Peter, L., et al. (2017). An immunogenic personal neoantigen vaccine for patients with melanoma. Nature *547*, 217–221.

Overwijk, W.W., Tsung, A., Irvine, K.R., Parkhurst, M.R., Goletz, T.J., Tsung, K., Carroll, M.W., Liu, C., Moss, B., Rosenberg, S.A., and Restifo, N.P. (1998). gp100/pmel 17 is a murine tumor rejection antigen: induction of "self"-reactive, tumoricidal T cells using high-affinity, altered peptide ligand. J. Exp. Med. *188*, 277–286.

Pai, C.S., Huang, J.T., Lu, X., Simons, D.M., Park, C., Chang, A., Tamaki, W., Liu, E., Roybal, K.T., Seagal, J., et al. (2019). Clonal Deletion of Tumor-Specific T Cells by Interferon-γ Confers Therapeutic Resistance to Combination Immune Checkpoint Blockade. Immunity *50*, 477–492.e8.

Reinhardt, J., Landsberg, J., Schmid-Burgk, J.L., Ramis, B.B., Bald, T., Glodde, N., Lopez-Ramos, D., Young, A., Ngiow, S.F., Nettersheim, D., et al. (2017). MAPK Signaling and Inflammation Link Melanoma Phenotype

Switching to Induction of CD73 during Immunotherapy. Cancer Res. *77*, 4697–4709.

Reinius, B., Mold, J.E., Ramsköld, D., Deng, Q., Johnsson, P., Michaëlsson, J., Frisén, J., and Sandberg, R. (2016). Analysis of allelic expression patterns in clonal somatic cells by single-cell RNA-seq. Nat. Genet. *48*, 1430–1435.

Riesenberg, S., Groetchen, A., Siddaway, R., Bald, T., Reinhardt, J., Smorra, D., Kohlmeyer, J., Renn, M., Phung, B., Aymans, P., et al. (2015). MITF and c-Jun antagonism interconnects melanoma dedifferentiation with pro-inflammatory cytokine responsiveness and myeloid cell recruitment. Nat. Commun. *6*, 8755.

Ritchie, M.E., Phipson, B., Wu, D., Hu, Y., Law, C.W., Shi, W., and Smyth, G.K. (2015). limma powers differential expression analyses for RNA-sequencing and microarray studies. Nucleic. Acids Res. *43*, e47, https://doi.org/10.1093/nar/gkv007.

Robinson, M.D., McCarthy, D.J., and Smyth, G.K. (2010). edgeR: a Bioconductor package for differential expression analysis of digital gene expression data. Bioinformatics *26*, 139–140.

Rodig, S.J., Gusenleitner, D., Jackson, D.G., Gjini, E., Giobbie-Hurder, A., Jin, C., Chang, H., Lovitch, S.B., Horak, C., Weber, J.S., et al. (2018). MHC proteins confer differential sensitivity to CTLA-4 and PD-1 blockade in untreated metastatic melanoma. Sci. Transl. Med. *10*, https://doi.org/10.1126/scitranslmed.aar3342.

Rosenberg, S.A., and Restifo, N.P. (2015). Adoptive cell transfer as personalized immunotherapy for human cancer. Science *348*, 62–68.

Sade-Feldman, M., Jiao, Y.J., Chen, J.H., Rooney, M.S., Barzily-Rokni, M., Eliane, J.-P., Bjorgaard, S.L., Hammond, M.R., Vitzthum, H., Blackmon, S.M., et al. (2017). Resistance to checkpoint blockade therapy through inactivation of antigen presentation. Nat. Commun. *8*, 1136.

Sahin, U., Derhovanessian, E., Miller, M., Kloke, B.-P., Simon, P., Löwer, M., Bukur, V., Tadmor, A.D., Luxemburger, U., Schrörs, B., et al. (2017). Personalized RNA mutanome vaccines mobilize poly-specific therapeutic immunity against cancer. Nature *547*, 222–226.

Schmid-Burgk, J.L., Schmidt, T., Gaidt, M.M., Pelka, K., Latz, E., Ebert, T.S., and Hornung, V. (2014). OutKnocker: a web tool for rapid and simple genotyping of designer nuclease edited cell lines. Genome Res. *24*, 1719–1723.

Schmid-Burgk, J.L., Höning, K., Ebert, T.S., and Hornung, V. (2016). CRISPaint allows modular base-specific gene tagging using a ligase-4-dependent mechanism. Nat. Commun. *7*, 12338.

Schumacher, T., Bunse, L., Pusch, S., Sahm, F., Wiestler, B., Quandt, J., Menn, O., Osswald, M., Oezen, I., Ott, M., et al. (2014). A vaccine targeting mutant IDH1 induces antitumour immunity. Nature *512*, 324–327.

Subramanian, A., Tamayo, P., Mootha, V.K., Mukherjee, S., Ebert, B.L., Gillette, M.A., Paulovich, A., Pomeroy, S.L., Golub, T.R., Lander, E.S., and Mesirov, J.P. (2005). Gene set enrichment analysis: a knowledge-based approach for interpreting genome-wide expression profiles. Proc. Natl. Acad. Sci. USA *102*, 15545–15550.

Takeda, K., Nakayama, M., Hayakawa, Y., Kojima, Y., Ikeda, H., Imai, N., Ogasawara, K., Okumura, K., Thomas, D.M., and Smyth, M.J. (2017). IFN-γ is required for cytotoxic T cell-dependent cancer genome immunoediting. Nat. Commun. *8*, 14607.

Tran, E., Robbins, P.F., Lu, Y.-C., Prickett, T.D., Gartner, J.J., Jia, L., Pasetto, A., Zheng, Z., Ray, S., Groh, E.M., et al. (2016). T-Cell Transfer Therapy Targeting Mutant KRAS in Cancer. N. Engl. J. Med. *375*, 2255–2262.

Verdegaal, E.M.E., de Miranda, N.F.C.C., Visser, M., Harryvan, T., van Buuren, M.M., Andersen, R.S., Hadrup, S.R., van der Minne, C.E., Schotte, R., Spits, H., et al. (2016). Neoantigen landscape dynamics during human melanoma-T cell interactions. Nature *536*, 91–95.

Verfaillie, A., Imrichova, H., Atak, Z.K., Dewaele, M., Rambow, F., Hulselmans, G., Christiaens, V., Svetlichnyy, D., Luciani, F., Van den Mooter, L., et al. (2015). Decoding the regulatory landscape of melanoma reveals TEADS as regulators of the invasive cell state. Nat. Commun. *6*, 6683.

Walton, S.M., Gerlinger, M., de la Rosa, O., Nuber, N., Knights, A., Gati, A., Laumer, M., Strauss, L., Exner, C., Schäfer, N., et al. (2006). Spontaneous CD8 T cell responses against the melanocyte differentiation antigen RAB38/NY-MEL-1 in melanoma patients. J. Immunol. *177*, 8212–8218.

Wang, R.F., Robbins, P.F., Kawakami, Y., Kang, X.Q., and Rosenberg, S.A. (1995). Identification of a gene encoding a melanoma tumor antigen recognized by HLA-A31-restricted tumor-infiltrating lymphocytes. J. Exp. Med. *181*, 799–804.

Wölfel, T., Hauer, M., Schneider, J., Serrano, M., Wölfel, C., Klehmann-Hieb, E., De Plaen, E., Hankeln, T., Meyer zum Büschenfelde, K.H., and Beach, D. (1995). A p16INK4a-insensitive CDK4 mutant targeted by cytolytic T lymphocytes in a human melanoma. Science *269*, 1281–1284.

Zaretsky, J.M., Garcia-Diaz, A., Shin, D.S., Escuin-Ordinas, H., Hugo, W., Hu-Lieskovan, S., Torrejon, D.Y., Abril-Rodriguez, G., Sandoval, S., Barthly, L., et al. (2016). Mutations Associated with Acquired Resistance to PD-1 Blockade in Melanoma. N. Engl. J. Med. *375*, 819–829.

Zhao, F., Sucker, A., Horn, S., Heeke, C., Bielefeld, N., Schrörs, B., Bicker, A., Lindemann, M., Roesch, A., Gaudernack, G., et al. (2016). Melanoma Lesions Independently Acquire T-cell Resistance during Metastatic Latency. Cancer Res. *76*, 4347–4358.

STAR★METHODS

KEY RESOURCES TABLE

REAGENT or RESOURCE	SOURCE	IDENTIFIER
Antibodies		
Mouse monoclonal β-Actin (Clone C4)	Santa Cruz	Cat# sc-47778; RRID:AB_2714189
Mouse monoclonal CDK4 (Clone DCS-35)	Santa Cruz	Cat#s c-23896; RRID:AB_627239
Rat monoclonal FLAG (Clone L5)	Novus	Cat# NBP1-06712; RRID:AB_1625981
Rabbit polyclonal MITF (Clone HPA003259)	Atlas Antibodies	Cat# HPA003259, RRID:AB_1079381
Mouse monoclonal RAB38 (A-8)	Santa Cruz	Cat# sc-390176; RRID: n/a
Mouse monoclonal TRP1 (G-9)	Santa Cruz	Cat# sc-166857; RRID:AB_1079381
IRDye 680RD Donkey anti-mouse IgG (H + L)	LI-COR Biosciences	Cat# 926-68072; RRID:AB_10953628
IRDye 800CW Donkey anti-rabbit IgG (H + L)	LI-COR Biosciences	Cat# 926-32213, RRID:AB_621848
IRDye 800CW Goat anti-rat IgG (H + L)	LI-COR Biosciences	Cat# 925-32219, RRID:AB_2721932
Anti-mouse CD16/CD32 (Clone 93)	BioLegend	Cat# 101302, RRID:AB_312801
Anti-mouse CD45.2 APC-Cy7 (Clone 104)	BioLegend	Cat# 109824,RRID:AB_830789
Anti-mouse CD45.1 Brilliant Violet 785 (Clone A20)	BioLegend	Cat# 110743,RRID:AB_2563379
Anti-mouse CD8a Brilliant Violet 711 (Clone 53-6.7)	BioLegend	Cat# 100747, RRID:AB_11219594
Anti-mouse CD8a PE (Clone 53-6.7)	BD Biosciences	Cat# 553033,RRID:AB_394571
Anti-mouse CD90.1 PerCP (Clone OX-7)	BD Biosciences	Cat# 557266, RRID:AB_396611
Anti-Mouse Vβ 13 TCR FITC (Clone MR12-3)	BD Biosciences	Cat# 553204,RRID:AB_394706
Anti-mouse Vα2 TCR Brilliant Violet 421 (Clone 20.1)	BD Biosciences	Cat# 562944
Anti-mouse CD69 APC (Clone H1.2F3)	Thermo Fisher Scientific	Cat# 17-0691-80, RRID:AB_1210796
Anti-mouse H-2D^{b} Biotin (KH95)	BD Biosciences	Cat# 553572, RRID:AB_394930
Anti-mouse H-2K^{b} Biotin (AF6-88.5)	BD Biosciences	Cat# 553568, RRID:AB_394926
Streptavidin APC	BD Biosciences	Cat# 554067, RRID:AB_10050396
Anti-mouse CD3e (Clone 145-2C11)	Tonbo Biosciences	Cat# 70-0031; RRID:AB_2621472
Anti-mouse CD28 (Clone 37.51)	Tonbo Biosciences	Cat# 70-0281; RRID:AB_2621492
Anti-mouse TNF-α APC (MP6-XT22)	BD Biosciences	Cat# 554420,RRID:AB_398553
Anti-mouse IFN-γ PE-Cy7 (XMG1.2)	BD Biosciences	Cat# 557649,RRID:AB_396766
Anti-mouse IFN-γ PE-Cy7 (XMG1.2)	Biolegend	Cat# 505826,RRID: 2295770
Annexin V APC	Biolegend	Cat# 640920; RRID: n/a
In vivo Mab rat anti-mouse PD-L1 (B7-H1) (Clone 10F.9G2)	Hölzel Biotech	Cat# BE0101; RRID:AB_10949073
In vivo Mab rat IgG2b isotype control (Clone LTF-2)	Hölzel Biotech	Cat# BE0090; RRID:AB_1107780
In vivo Mab anti-mouse TNF alpha (Clone XT3.11)	Hölzel Biotech	Cat# BE0058; RRID:AB_1107764
In vivo Mab anti-mouse IFN gamma (Clone XMG1.2)	Hölzel Biotech	Cat# BE0055; RRID:AB_1107694
Bacterial and Virus Strains		
Recombinant adenoviral vector Ad-hgp100	Landsberg et al., 2012	N/A
Chemicals, Peptides, and Recombinant Proteins		
Cyclophosphamide	Endoxan, Baxter	Cat# 01469644
Poly(I:C) (HMW)	Invivogen	Cat# tlrl-pic
H2-D^{b} binding peptide KVPRNQDWL (hgp100$_{25-33}$)	JPT	N/A
H2-K^{b} binding protein SSIEFARL (HSV-1 gB$_{498-505}$)	GenScript	N/A
Recombinant human IL-2 (Aldesleukin)	Novartis Pharma	PZN: 02238131
Recombinant murine IFN-γ	Peprotech	Cat# 315-05
Recombinant murine TNF-α	Peprotech	Cat# 315-01A

(*Continued on next page*)

Continued

REAGENT or RESOURCE	SOURCE	IDENTIFIER
BD GolgiPlug (Protein Transport Inhibitor; containing Brefeldin A)	BD Biosciences	Cat# 555029
Brefeldin A	Sigma-Aldrich	Cat# B7651
Propidium iodide solution	Biolegend	Cat# 421301
Annexin V binding buffer	Biolegend	Cat# 422201
Q5 DNA polymerase	NEB	Cat# M0491
DAPI	Thermo Fisher Scientific	Cat#D1306; RRID:AB_2629482
TRIzol reagent	Invitrogen	Cat# 15596026
BpiI (BbsI)	Thermo Fisher Scientific	Cat# ER1011
Critical Commercial Assays		
Cytofix/Cytoperm Fixation /Permeabilization Solution Kit	BD Biosciences	Cat#554714
NucleoSpin® Tissue kit	Macherey-Nagel	Cat#740952
NucleoSpin® RNA kit	Macherey-Nagel	Cat#740955
Deposited Data		
Raw data 3′mRNA-Seq	ENA (European Nucleotide Archive)	PRJEB30997 PRJEB37461 PRJEB37462
Experimental Models: Cell Lines		
Mouse: HCmel12 melanoma	Established in the laboratory of T.T. (Bald et al., 2014a)	N/A
Mouse: HC.*Pmel*$^{-/-}$.	This paper	N/A
Mouse: HC.*Pmel*$^{-/-}$.TYRP1-mNeon	This paper	N/A
Mouse: HC.*Pmel*$^{-/-}$.TYRP1-NFhgp100	This paper	N/A
Mouse: HC.*Pmel*$^{-/-}$.RAB38-mNeon	This paper	N/A
Mouse: HC.*Pmel*$^{-/-}$. RAB38-NFhgp100	This paper	N/A
Mouse: HC.*Pmel*$^{-/-}$.CDK4^{R24C}-mNeon	This paper	N/A
Mouse: HC.*Pmel*$^{-/-}$.CDK4^{R24C}-NFhgp100	This paper	N/A
Mouse: HC.*Pmel*$^{-/-}$.DCT-NFhgp100	This paper	N/A
Mouse: HC.*Pmel*$^{-/-}$.DCT-mNeon	This paper	N/A
Mouse: HC.*Pmel*$^{-/-}$.GPNMB-NFhgp100	This paper	N/A
Mouse: HC.*Pmel*$^{-/-}$.GPNMB-mNeon	This paper	N/A
Mouse: HC.*Pmel*$^{-/-}$.SOX10-NFhgp100	This paper	N/A
Mouse: *HC.Pmel*$^{-/-}$.SOX10-mNeon	This paper	N/A
Mouse: HC.*Pmel*$^{-/-}$.TYRP1-mScarlet	This paper	N/A
Mouse: HC.*Pmel*$^{-/-}$.TYRP1-SFmgp100	This paper	N/A
Mouse: HC.*Pmel*$^{-/-}$.TYRP1-SFhgp100	This paper	N/A
Mouse: B16 melanoma	Obtained by T.T. from ATCC	ATCC CRL-6323
Mouse: B16.ACTB-mNeon	This paper	N/A
Mouse: B16.ACTB-NFgB	This paper	N/A
Mouse: B16.ACTB-mScarlet	This paper	N/A
Mouse: B16.ACTB-SFgB	This paper	N/A
Mouse: B16.ACTG1-mNeon	This paper	N/A
Mouse: B16.ACTG1-NFgB	This paper	N/A
Experimental Models: Organisms/Strains		
Mouse:C57BL/6J (H-2D^{b})	Janvier LABS	Cat#Sc-C57J
Mouse:C57BL/6J (H-2D^{b})	Charles River	Cat#JAX 000664
Mouse:C57BL/6J (H-2D^{b})	The Peter Doherty Institute for Infection and Immunity	N/A
Mouse: pmel-1TCRtg	Jackson Laboratory	Cat#005023

(*Continued on next page*)

Continued

REAGENT or RESOURCE	SOURCE	IDENTIFIER
Mouse: gBT-I TCRtg	The Peter Doherty Institute for Infection and Immunity	N/A
Oligonucleotides		
CPG Oligo 1826; 5′- 3' T*C*C*A*T*G*A*C*G*T*T*C*C*T*G*A*C*G*T*T-3′	Biomers	N/A
P1/P2_forward CAAGAATGAAGCCAACCAGCC	Microsynth	N/A
P3_forward GAACCGGACATTGTGAAGCC	Microsynth	N/A
P4_forward GAATCTCTGCCTTCCGAGCC	Microsynth	N/A
P1/P4_reverse CGCTTGCCATTTCCAGTGG	Microsynth	N/A
P2/P3_reverse GTTAGCAGACTTCCTCTGCCC	Microsynth	N/A
Actb_forward CCAGTTGGTAACAATGCCATGT	Microsynth	N/A
Actb_reverse GGCTGTATTCCCCTCCATCG	Microsynth	N/A
Pmel_TS CACCGCTTGTGCTGAGTGCTCTGC	Microsynth	N/A
Pmel_BS AAACGCAGAGCACTCAGCACAAGC	Microsynth	N/A
Tyrp1_TS CACCGGCAGGCGGCTATCAGACCA	Microsynth	N/A
Tyrp1_BS AAACTGGTCTGATAGCCGCCTGCC	Microsynth	N/A
Rab38_TS CACCGTGGCTGTGCCAAATCCTAGA	Microsynth	N/A
Rab38_BS AAACTCTAGGATTTGGCACAGCCAC	Microsynth	N/A
Cdk4_TS CACCGCACTCCTACCTGCACAAGG	Microsynth	N/A
Cdk4_BS AAACCCTTGTGCAGGTAGGAGTGC	Microsynth	N/A
Dct_TS CACCGCAGCAGCAAGAGATACACGG	Microsynth	N/A
Dct_BS AAACCCGTGTATCTCTTGCTGCTGC	Microsynth	N/A
Gpnmb_TS CACCGCCAAAGACTTAGAGTGTCCT	Microsynth	N/A
Gpnmb_BS AAACAGGACACTCTAAGTCTTTGGC	Microsynth	N/A
Sox10_TS CACCGACTCTATCCCGACCTTAGAG	Microsynth	N/A
Sox10_BS AAACCTCTAAGGTCGGGATAGAGTC	Microsynth	N/A
Actb_TS CACCGCACCGCAAGTGCTTCTAGG	Microsynth	N/A
Actb_BS AAACCCTAGAAGCACTTGCGGTGC	Microsynth	N/A
Actg1_TS CACCGCCACCGCAAATGCTTCTAGA	Microsynth	N/A

(*Continued on next page*)

Continued

REAGENT or RESOURCE	SOURCE	IDENTIFIER
Actg1_BS AAACTCTAGAAGCATTTGCGGTGGC	Microsynth	N/A
Recombinant DNA		
px330-U6-Chimeric_BB-CBh-hSPCas9	Addgene	Cat#42230
pCAS9-mCherry-Frame +0	Addgene	Cat#66939
pCAS9-mCherry-Frame +1	Addgene	Cat #66940
pCAS9-mCherry-Frame +2	Addgene	Cat #66941
pCRISPaint-mNeon-PuroR	Veit Hornnung	N/A
pmScarlet_C1	Addgene	Cat#85042
px330_*Pmel*$^{-/-}$-sgRNA	This paper	N/A
pRP-GFP	Eike Latz	N/A
px330_Tyrp1_Ct	This paper	N/A
px330_Rab38_Ct	This paper	N/A
px330_Cdk4_Ct	This paper	N/A
px330_Dct_Ct	This paper	N/A
px330_Gpnmb_Ct	This paper	N/A
px330_Sox10_Ct	This paper	N/A
px330_Actb_Ct	This paper	N/A
px330_Actg1_Ct	This paper	N/A
pCRISPaint-mNeon-PuroR [M1G]	This paper	N/A
pCRISPaint-mNeon-F-hgp100-PuroR [M1G]	This paper	N/A
pCRISPaint-mNeon-F-mgp100-PuroR [M1G]	This paper	N/A
pCRISPaint-mNeon-F-gB-PuroR [M1G]	This paper	N/A
pCRISPaint-mNeon-F-Ova-PuroR [M1G]	This paper	N/A
pCRISPaint-mNeon-BlastR [M1G]	This paper	N/A
pCRISPaint-mNeon-F-hgp100-BlastR [M1G]	This paper	N/A
pCRISPaint-mNeon-F-mgp100-BlastR [M1G]	This paper	N/A
pCRISPaint-mNeon-F-gB-BlastR [M1G]	This paper	N/A
pCRISPaint-mNeon-F-Ova-BlastR [M1G]	This paper	N/A
pCRISPaint-mScarlet-PuroR [M1G]	This paper	N/A
pCRISPaint-mScarlet-F-hgp100-PuroR [M1G]	This paper	N/A
pCRISPaint-mScarlet-F-mgp100-PuroR [M1G]	This paper	N/A
pCRISPaint-mScarlet-F-gB-PuroR [M1G]	This paper	N/A
pCRISPaint-mScarlet-F-Ova-PuroR [M1G]	This paper	N/A
pCRISPaint-mScarlet-BlastR [M1G]	This paper	N/A
pCRISPaint-mScarlet-F-hgp100-BlastR [M1G]	This paper	N/A
pCRISPaint-mScarlet-F-mgp100-BlastR [M1G]	This paper	N/A
pCRISPaint-mScarlet-F-gB-BlastR [M1G]	This paper	N/A
pCRISPaint-mScarlet-F-Ova-BlastR [M1G]	This paper	N/A
Software and Algorithms		
FlowJo v10	Tree Star, Inc.	https://flowjo.com/
Prism v8	GraphPad	https://www.graphpad.com/scientific-software/prism/
FIJI package	ImageJ	https://fiji.sc/
ZEN software	Zeiss	https://www.zeiss.de
Adobe Illustrator v24.1	Adobe	https://www.adobe.com/
Adobe Acrobat Pro DC	Adobe	https://www.adobe.com/
R	R developer team	https://cran.r-project.org/
Rstudio	Rstudio	https://www.rstudio.com/

(*Continued on next page*)

Continued

REAGENT or RESOURCE	SOURCE	IDENTIFIER
Bioconductor - R-based computing platform	Bioconductor developer team	https://doi.org/10.18129/B9.bioc.edgeR
Rsubread - Bioconductor package	Liao et al., 2013	https://doi.org/10.18129/B9.bioc.Rsubread
edgeR - Bioconductor package	Robinson et al., 2010	https://doi.org/10.18129/B9.bioc.edgeR
org.Mm.eg.db - Bioconductor package, Genome wide annotation for Mouse. R package version 3.4.1.	Package author: Carlson, M.	https://doi.org/10.18129/B9.bioc.org.Mm.eg.db
heatmap.3 - An Improved Heatmap Package. R package.	Package authors: Zhao, S., Guo, Y., Sheng, Q., Shyr, Y.	https://www.rdocumentation.org/packages/GMD/versions/0.3.3/topics/heatmap.3
Voom - algorithm (implemented in limma)	Law et al., 2014	https://doi.org/10.18129/B9.bioc.limma
RNA-seq algorithm	As described by Shi et al., Bioinformatics Division, WEHI, Melbourne, Australia	http://bioinf.wehi.edu.au/RNAseqCaseStudy/
limma	Ritchie et al., 2015	https://doi.org/10.18129/B9.bioc.limma
Beeswarm	R-package author: Aron Eklund	http://CRAN.R-project.org/package=beeswarm
GSEA (Gene set enrichment analysis)	GSEA Subramanian et al. (2005, PNAS 102, 15545-15550).	https://www.gsea-msigdb.org/gsea/index.jsp

RESOURCE AVAILABILITY

Lead contact

Further information and requests for reagents may be directed to, and will be fulfilled by the Lead Contact Michael Hölzel (michael.hoelzel@ukbonn.de).

Materials availability

Newly generated plasmids and cell lines are available upon request. Requests may be directed to, and will be fulfilled by the Lead Contact Michael Hölzel (michael.hoelzel@ukbonn.de).

Data and code availability

Original raw 3′mRNA-Seq data have been deposited to EBI ENA under the study accession numbers PRJEB30997, PRJEB37461 and PRJEB37462.

EXPERIMENTAL MODEL AND SUBJECT DETAILS

Mice

C57BL/6J (H-2D^b) mice were purchased from Janvier Labs or Charles River Laboratories or the Walter and Eliza Hall Institute for Medical Research (Melbourne, Australia), bred in the Peter Doherty Institute for Infection and Immunity (Melbourne, Australia) or the QIMR Berghofer Medical Research Institute (Herston, Australia) TCR-transgenic pmel-1 mice expressing an αβ TCR recognizing the amino acids 25-33 of human or the amino acids 25-33 of mouse gp100 presented by H-2D^b were bred as described previously (Glodde et al., 2017; Landsberg et al., 2012). TCR-transgenic gBT-I mice expressing an αβ TCR recognizing the amino acids 498-505 of HSV-1 glycoprotein B were bred in the Peter Doherty Institute for Infection and Immunity (Melbourne, Australia) as described (Macleod et al., 2014). All animals were bred and maintained in individually ventilated cages under specific pathogen-free conditions. Experiments were performed with 6 - 10 old week mice. At the start of the experiment, age and sex matched mice were randomly allocated to different experimental groups. All animal experiments were approved by the local government authorities (LANUV, NRW, Germany; The University of Melbourne Animal Ethics Committee and QIMR Berghofer AEC, Queensland, Australia) and performed in adherence to the national and institutional guidelines for the care and use of laboratory animals.

Cell lines

The melanoma cell line HCmel12 was established from a primary melanoma in the *Hgf-CDK4^{R24C}* mouse model by serial transplantation in our laboratory as previously described (Bald et al., 2014a). The *Pmel* gene was inactivated using the CRISPR-Cas9 technology to generate the HC.*Pmel*$^{-/-}$ melanoma monoclonal cell line. The B16F1 melanoma cell line was originally obtained from ATCC by T. Tüting. All melanoma cell lines were routinely cultured in RPMI 1640 medium supplemented with 10% FCS, 2 mM L-glutamine, 10 mM non-essential amino acids, 1 mM HEPES, 20 μM β-Mercaptoethanol, 100 IU ml^{-1} penicillin and 100 μg ml^{-1} streptomycin

(all by Life Technologies) in a humidified incubator with 5% CO_2 at 37°C. All cell lines used in this study were routinely tested for Mycoplasma contamination by PCR.

Primary cell cultures

Ex vivo cell cultures were established from all transplanted non-treated and esACT-recurrent melanomas. Tumor tissue was harvested, dissociated mechanically and incubated with 1 mg ml^{-1} Collagenase D (Sigma) and 1 mg ml^{-1} DNase I (Roche) in PBS supplemented with 5% FCS (Biochrom) for 30 min at 37°C and subsequently passed through a 70 μm cell strainer (BD Bioscience). After washing, single tumor cell suspensions were cultured in RPMI 1640 medium supplemented with 10% FCS, 2 mM L-glutamine, 10 mM non-essential amino acids, 1 mM HEPES, 20 μM β-Mercaptopethanol, 100 IU ml^{-1} penicillin and 100 μg ml^{-1} streptomycin (all by Life Technologies) in a humidified incubator with 5% CO_2 at 37°C. All cell lines were analyzed for mNeon expression by flow cytometry immediately after isolation and two weeks after *ex vivo* culture.

For *in vitro* studies, single cell suspensions of TCR-transgenic (TCRtg) T cells isolated from spleens of pmel-1 or gBT-I TCRtg mice were cultured in RPMI 1640 medium supplemented with 10% FCS, 2 mM L-glutamine, 10 mM non-essential amino acids, 1 mM HEPES, 20 μM β-Mercaptopethanol, 100 IU ml^{-1} penicillin, 100 μg ml^{-1} streptomycin (all by Life Technologies) and 12.5 - 100 U ml^{-1} recombinant IL-2 (Novartis Pharma or Peprotech; see individual methods) in a humidified incubator with 5% CO_2 at 37°C.

METHOD DETAILS

Generation of CRISPitope plasmids

The plasmid px330-U6-Chimeric_BB-CBh-hSPCas9 was used as target selector. To generate various target selectors, the plasmid was digested with the restriction enzyme BbsI (NEB) and gel purified. A double-stranded DNA oligonucleotide targeting the C terminus of the desired target gene was cloned into the BbsI-digested px330 to generate a functional sgRNA. px330-U6-Chimeric_BB-CBh-hSPCas9 was a gift from Feng Zhang (Addgene, plasmid #42230). Frame selectors pCAS9-mCherry-Frame +0, pCAS9-mCherry-Frame +1 and pCAS9-mCherry-Frame +2 were a gift from Veit Hornung (Addgene, plasmids #66939, #66940 and #66941). Universal donor plasmids used in this study were cloned based on the pCRISPaint-mNeon-PuroR plasmid described by Schmid-Burgk and colleagues (Schmid-Burgk et al., 2016). The universal donor pCRISPaint-mNeon-PuroR was a gift from Veit Hornung (LMU, Munich, Germany). Using molecular cloning approaches, the pCRISPaint-mNeon-PuroR plasmid was further modified by (1) exchanging the Puromycin resistance cassette by a Blasticidin resistance cassette, (2) exchanging the Methionine start codon (ATG) of the resistance cassettes by a Glycine (GGG) to prevent transcription from random genomic integrations, (3) exchanging the mNeon fluorescent protein by the mScarlet fluorescent protein, and (4) addition of a FLAG-tag and one of four immunological epitope tags [KVPRNQDWL ($hgp100_{25-33}$), EGSRNQDWL ($mgp100_{25-33}$), SIINFEKL ($Ova_{257-264}$) or SSIEFARL (HSV-1 $gB_{498-505}$), to the fluorescent protein (C terminus). The mScarlet-coding sequence was amplified from the plasmid pmScarlet_C1. The plasmid pmScarlet_C1 was a gift from Dorus Gadella (Addgene, plasmid #85042).

Generation of HC.*Pmel*$^{-/-}$ cell line

To stably inactivate the *Pmel* gene, HCmel12 melanoma cells were targeted by CRISPR-Cas9. Therefore, the plasmid px330-U6-Chimeric_BB-CBh-hSPCas9 (Addgene, plasmid #42230) was digested with the restriction enzyme BpiI (Thermo Fisher Scientific) and gel purified. A double-stranded DNA oligonucleotide targeting upstream of the genomic region encoding for the pmel-1 T cell epitope in exon 1 of the murine *Pmel* gene was cloned into the BpiI-digested plasmid to generate a functional sgRNA. For plasmid transfection, 5 × 10^5 HCmel12 melanoma cells were seeded in a 12-well plate 2 h prior to transfection. The cells were transfected with 2 μg of plasmid DNA (mix of 1.6 μg px330-*Pmel*$^{-/-}$-sgRNA and 0.4 μg pRP-GFP) in OptiMEM I (Life Technologies) using 0.6 μl FuGENE® HD transfection reagent (Promega) according to the manufacturer's instructions. Two days post transfection, GFP-positive cells were sorted using a FACS Aria III high-speed cell sorter (BD) and plated at single cell concentration (0.7 cells per 96 well). Genomic aberrations of *Pmel*$^{-/-}$ single cell clones were characterized by next generation sequencing and analyzed using the web tool OutKnocker (Schmid-Burgk et al., 2014).

Generation of CRISPitope-engineered cell lines

CRISPitope-engineered melanoma cell lines were generated by targeting the C-termini of various target genes by CRISPR-assisted insertion of epitopes. For CRISPitope plasmid transfection, 5 × 10^4 – 1 × 10^5melanoma cells were seeded in a 96-well plate and transfected with 200 ng of DNA (50 ng target selector, 50 ng frame selector and 100 ng universal donor) in Opti-MEM I (Life Technologies) using 0.6 μl of FuGENE® HD transfection reagent (Promega) according to the manufacturer's instructions. Two days post transfection, HC.*Pmel*$^{-/-}$ cells were selected with 2 μg ml^{-1} Puromycin (Sigma-Aldrich) for 3 days and B16 cells were selected with 10 μg ml^{-1} l Blasticidin S (Sigma-Aldrich) for 7 days. After selection, CRISPitope-engineered cell lines were sorted for mNeon or mScarlet expression, using a FACS Aria III high-speed cell sorter (BD) and subsequently polyclonal cultures of the individual cell lines were established.

Western blotting

Protein lysates were prepared by lysing cultured melanoma cells in 1xLaemmli buffer (4% SDS, 20% Glycerol, 120 mM Tris-HCl pH 6.8, 0.02% bromophenol blue, 20 mM DTT) and incubation at 95°C for 5 min. Total cell lysates were separated by 10% SDS-PAGE gel

electrophoresis and transferred to a nitrocellulose membrane (pore size: 0.2 μm; GE Healthcare) according to standard procedures. After 1 h of blocking with 5% bovine serum albumin (GE Healthcare) in TBS with 0.5% Tween-20, membranes were incubated with primary antibodies overnight at 4°C. Blots were immunostained with β-Actin (C4, Santa Cruz sc-47778, 1:2,000, mouse mAb), CDK4 (DCS-35, Santa Cruz sc-23896, 1:100, mouse mAb), FLAG (L5, Novus Biologicals NBP2-06712, 1:500, rat mAb), MITF (HPA003259, Atlas Antibodies, Sigma-Aldrich, 1:250; rabbit poAb), RAB38 (A-8, Santa Cruz sc-390176, 1:100, mouse mAb) and TRP1 (G-9, Santa Cruz sc-166857, 1:100, mouse mAb). These proteins were detected using corresponding donkey anti-mouse IRDye 680 LT, donkey anti-rabbit IRDye 800 CW or donkey anti-rat IRDye 800 (all by LI-COR Biosciences, 1:15,000) secondary antibodies and scanned with the Odyssey Sa Imaging system (LI-COR Biosciences).

Epifluorescence microscopy

Melanoma cells were seeded on coverslips overnight and fixed in 4% p-formaldehyde (Carl Roth) in PBS for 4 min at room temperature. After washing, cells were permeabilized using 0.04% Triton X-100 (Sigma-Aldrich) in PBS for 5 min at room temperature, washed and incubated with 0.5 μg ml^{-1} DAPI (4,6-diamindino-2-phenylindole; Thermo Scientific) in PBS for 1 min. After washing, cells were mounted on objective slides using Fluoroshield mounting medium (Sigma-Aldrich). Epifluorescence microscopy was performed using a Carl Zeiss Observer Z1 (40 x oil-immersion objective). Data were processed using Carl Zeiss Zen software and ImageJ (Fiji package).

In vitro pmel-1 T cell activation assay

Antigen-dependent T cell activation in the presence of melanoma cells was assessed by flow cytometry using either CD69 surface expression on the pmel-1 TCRtg T cells or intracellular expression the cytokine IFN-γ and TNF-α. For both assays, melanoma cells were stimulated with murine recombinant IFN-γ (10 U ml^{-1} or 1000 U ml^{-1}; Peprotech) for 72 h and analyzed for H-$2D^b$ surface expression. Pmel-1 TCRtg T cells were isolated from naive mice and the frequency of antigen-specific T cells was determined using flow cytometry and the surface markers CD8, CD90.1 and Vβ13 TCR. In order to assess CD69 surface expression of pmel-1 TCRtg T cells isolated from naive mice, the pmel-1 TCRtg T cells were co-cultured with melanoma cells (ratio 1: 1.5) for 16 h in "complete" RPMI 1640 medium supplemented with recombinant human IL-2 (30 U ml^{-1}; Aldesleukin; Novartis Pharma) in 96 well-plates. T cell activation was assessed by the expression of the surface marker CD69 using flow cytometry. In order to measure T cell activation by the expression of the intracellular cytokines IFN-γ and TNF-α, pmel-1 TCRtg T cells were activated *in vitro* and subsequently co-cultured with the CRISPitope-engineered melanoma cells. For *in vitro* activation, 1 × 10^6 ml^{-1} pmel-1 TCRtg were cultured in "complete" RPMI 1640 supplemented with recombinant human IL-2 (100 U ml^{-1}; Aldesleukin; Novartis Pharma) and recombinant $hgp100_{25-33}$ peptide (1 μg ml^{-1}, JPT) for 5 days. The cells were split on day 2, 3 and 4 and the media was additionally supplemented with recombinant human IL-2 (100 U ml^{-1}; Aldesleukin; Novartis Pharma). After determining the amount of antigen-specific T cells, melanoma cells and T cells were co-cultured (ratio 1:0.25) in medium supplemented with GolgiPlug (1:1000, BD Biosciences) for 5 h. Intracellular staining was carried out using the Fixation/Permeabilization Solution Kit (BD Biosciences) according to manufacturer's protocols. Single cell suspensions were stained with antibodies against cell-surface antigens, fixed and permeabilized followed by intracellular staining with anti-mouse TNF-α (Clone MP6-XT22, BD Biosciences) and anti-mouse IFN-γ (Clone XMG1.2, BD Biosciences). All data were acquired with a FACS Canto II or LSR Fortessa flow cytometer (BD Biosciences) and analyzed using FlowJo v10 software for Windows (Tree Star, Inc.).

In vitro gBT-I T cell activation assay

Five days prior to the assay, gBT-I and C57BL/6 mice were sacrificed and the spleens were harvested. Individual single cell suspensions of the spleens were prepared. Splenocytes from C57BL/6 mice were pulsed with 0.1 μg ml^{-1} SSIEFARL peptide (GenScript) for 45 min at 37°C. After washing, 6 μg LPS (Sigma Aldrich) in a total volume of 10 mL complete PRMI medium was added to the splenocytes. Half of the gBT-I splenocytes were mixed with half of the peptide-pulsed C57BL/6 splenocytes in a total volume of 40 mL complete RPMI medium and incubated in a humidified incubator at 37°C. On day 2, 3 and 4 cells were split (1:2) and stimulated with recombinant human IL-2 (final concentration 12.5 IU ml^{-1}; Peprotech). To determine the number of T cells specific for the gB epitope, day 5 *in vitro* activated gBT-I T cells were stained for CD45.1, CD8 and Vα2 and analyzed by flow cytometry. One day prior to the co-culture assay, melanoma cells were stimulated with murine recombinant IFN-γ (0.1 ng ml^{-1}; Peprotech) for 18 h and analyzed for H-$2K^b$ surface expression by flow cytometry. After determining the amount of gB-specific T cells, melanoma cells and T cells were co-cultured (ratio 1:0.5) in medium supplemented with 10 μg ml^{-1} Brefeldin A (Sigma-Aldrich) for 5 h. Intracellular staining was carried out using the Fixation/Permeabilization Solution Kit (BD Biosciences) according to manufacturer's protocols. Single cell suspensions were stained with antibodies against cell-surface antigens, fixed and permeabilized followed by intracellular staining with anti-mouse TNF-α (Clone MP6-XT22, BD Biosciences) and anti-mouse IFN-γ (Clone XMG1.2, BD Biosciences). All data were acquired using a LSR Fortessa flow cytometer (BD Biosciences) and analyzed using FlowJo v10 software for Windows (Tree Star, Inc.).

Tumor transplantation experiments

Cohorts of syngeneic C57BL/6 mice were injected with either 2 × 10^5 HC.*Pmel*$^{-/-}$, HC.*Pmel*$^{-/-}$.TYRP1-NFhgp100, HC.*Pmel*$^{-/-}$.Rab38-NFhgp100, HC.*Pmel*$^{-/-}$.CDK4^{R24C}-NFhgp100 or respective HC.*Pmel*$^{-/-}$.mNeon control melanoma cells (HC.*Pmel*$^{-/-}$.TYRP1-mNeon, HC.*Pmel*$^{-/-}$.RAB38-mNeon or HC.*Pmel*$^{-/-}$.CDK4^{R24C}-mNeon) in 100 μl PBS intradermally (i.d.) into the flanks. Tumor size was measured twice weekly and recorded as mean tumor diameter in millimeters. Tumor area was calculated

by using the following equation: A = width x length [mm^2]. Mice were sacrificed when tumors exceeded 100 mm^2 or when signs of illness were observed.

Adoptive cell transfer (ACT) immunotherapy

ACT (esACT) immunotherapy was performed as previously described (Glodde et al., 2017). Briefly, when transplanted parental and CRISPitope-engineered melanomas reached a size of 3-5 mm in diameter mice were treated with the established ACT immunotherapy. Mice were pre-conditioned for ACT by a single intraperitoneal (i.p.) injection of 2 mg kg^{-1} KG cyclophosphamide (Endoxan) in 100 µl PBS one day prior to intravenous injection of 2 × 10^6 gp100-specific $CD8^+$ $CD90.1^+$ Vβ 13 TCR^+ pmel-1 T cells (in 100 µl PBS) isolated from spleens of naive pmel-1 TCR transgenic mice. The transferred T cells were activated *in vivo* by a single i.p. injection of 5 × 10^8 plaque forming units (PFU) of a recombinant adenoviral vector Ad-gp100 (in 100 µl PBS). On day 3, 6 and 9 after adoptive pmel-1 T cell transfer, 50 µg of CpG 1826 (MWG Biotech) and 50 µg of Poly(I:C) (polyinosinic:polycytidylic acid, Invivogen) in 100 µl distilled water were injected intratumorally. Cohorts of mice (indicated within the manuscript) were also treated with a modified ACT treatment regimen which does not include the administration of the adenovirus Ad-hgp100.

Salvage immune checkpoint inhibition therapy

When esACT-recurrent HC.*Pmel*$^{-/-}$.$CDK4^{R24C}$-NFhgp100 melanomas reached a size of ≥ 4 mm in diameter, anti-PD-L1 (αPD-L1) salvage therapy was started. Therefore, mice received two cycles of twice weekly i.p. injections with 250 µg rat anti-mouse PD-L1 (Clone 10F.9G2; Hölzel Biotech, Germany) in 100 µl PBS.

Concomitant ACT and checkpoint immunotherapy

C57BL/6 mice inoculated with HC.*Pmel*$^{-/-}$.$CDK4^{R24C}$-NFhgp100 were treated concomitantly with ACT and αPD-L1 immunotherapy when transplanted melanomas reached a size of 3-5 mm in diameter. Mice received the standard ACT treatment regimen as described above and were additionally treated with 250 µg rat anti-mouse PD-L1 (Clone 10F.9G2; Hölzel Biotech, Germany) or isotype control in 100 µl PBS on days 3, 6, 9 and 12 after T cell transfer.

Tissue digestion and processing

Tumor tissues, lymph nodes and spleens were harvested, dissociated mechanically and incubated with 1 mg ml^{-1} Collagenase D (Sigma), 1 mg ml^{-1} DNase I (Roche) and 5% FCS in PBS for 30 min at 37°C. Tissues were passed through a 70 µm cell strainer (Falcon) and single cell suspensions were washed twice with PBS. To remove erythrocytes, blood and spleen tissue suspensions were incubated with erythrocyte lysis buffer (0.1 mM Disodium-EDTA pH 7.3, 155 mM NH_4Cl, 10 mM $KHCO_3$) for 5 min and washed twice with PBS before further processing.

Flow cytometry

Immunostainings were performed according to standard protocols. Single cell suspensions were stained with the following fluorochrome-conjugated antibodies: anti-mouse CD45.2 (104, Biolegend, 1:100), anti-mouse CD45.1 (A20, Biolegend, 1:100), anti-mouse CD8 (53-6.7, Biolegend, 1:100), anti-mouse CD90.1 (OX-7, BD Biosciences, 1:100), anti-mouse Vβ 13 TCR (MR12-3, BD Biosciences, 1:50), anti-mouse Vα2 TCR (B20.1, BD Horizon, 1:200) and anti-mouse CD69 (H1.2F3, eBioscience, 1:100) in FACS buffer (2 mM EDTA, 2% FCS in PBS). Intracellular staining was carried out using the Fixation/Permeabilization Solution Kit (BD Biosciences) according to manufacturer's protocols. Single cell suspensions were stained with antibodies against cell surface antigens, fixed and permeabilized followed by intracellular staining with anti-mouse TNF-α (BD PharMingen, 1:100) and anti-mouse IFN-γ (XMG1.2, BD PharMingen or Biolegend, 1:100). Cultured melanoma cells were analyzed for endogenous mNeon or mScarlet expression and stained with anti-H-$2D^b$ (KH954, BD Biosciences, 1:50) or anti-H-$2K^b$ (AF6-88.5, BD Biosciences, 1:50) and corresponding Streptavidin (BD-Bioscience, #554067, 1:100) for the analyses of MHC class I surface expression. All data were recorded on a FACS Canto II or LSR Fortessa flow cytometer (BD Biosciences) and analyzed using FlowJo v10 software for Windows (Tree Start, Inc.).

PCR analysis of recurrent melanomas

Genomic DNA (gDNA) from cultured melanoma cells or tissue was extracted using the NucleoSpin® Tissue kit (Macherey-Nagel) according to the manufacturer's instructions. gDNA was used as template for the amplification of the desired target region by PCR using Q5 DNA polymerase (NEB). PCR amplicons were visualized by agarose gel electrophoresis and analyzed by Sanger sequencing (Microsynth, Switzerland).

Melanoma cell dedifferentiation assay

Melanoma cells were dedifferentiated using either T cell–conditioned media (TCM) or cytokines. For generation of TCM, splenocytes of naive C57BL/6 mice were activated using anti–mouse CD3ε+CD28 stimulation. Multi-well plates were coated with 10 µg ml^{-1} anti-mouse CD3ε antibody (Clone 145-2C11, Tonbo Biosciences) in 50 µl PBS overnight at 4°C and washed twice before adding cells. Splenocytes were seeded into the wells at a density of 1x10^6 cells ml^{-1} and stimulated with 2 µg ml^{-1} anti-mouse CD28 (Clone 37.51, Tonbo Biosciences) in "complete" RPMI medium for 60 h. CRISPitope-modified melanoma cells were treated with the diluted supernatant (dilution 1:2 with "complete" RPMI 1640) and analyzed for mNeon expression by flow cytometry after 5 days. Media was

changed every second day. For the dedifferentiation of melanoma cells using cytokines, indicated melanoma cells were treated with 500 U ml^{-1} of murine recombinant IFN-γ and/or TNF-α (both by Peprotech) for 5 days and subsequently analyzed for mNeon expression by flow cytometry. Media was changed daily. All data was recorded on a FACS Canto II or LSR Fortessa flow cytometer (BD Biosciences) and analyzed using FlowJo v10 software for Windows (Tree Start, Inc.).

Apoptosis assay

Melanoma cells were treated with TCM as described above. Additionally, the TCM was supplemented with αIFN-γ (10 μg ml^{-1}, XMG1.2, Hölzel Biotech) and/or αTNF-α (10 μg ml^{-1}, Clone XT3.11, Hölzel Biotech). After 5 days of treatment, apoptosis was analyzed using an Annexin V Apoptosis Kit (Biolegend) by flow cytometry according to the user manual. All data was recorded on a FACS Canto II or LSR Fortessa flow cytometer (BD Biosciences) and analyzed using FlowJo v10 software for Windows (Tree Start, Inc.).

3′mRNA-Seq analysis of melanomas

Total RNA from homogenized melanoma tissues were extracted using TRIzol reagent (Thermo Fisher) and the NucleoSpin® RNA kit (Macherey Nagel) according to manufacturer's recommendations. RNA concentrations were determined using a *NanoDrop* Spectrophotometer (PeqLab, Germany). 3′mRNA-seq library preparation was performed using the forward QuantSeq 3′mRNA-Seq Library Prep Kit for Illumina (Lexogen GmbH, Austria) according to the manufacturer's protocol. Size distribution and yield of the library after the PCR step was determined by the D1000 high sensitivity tape station (Agilent) prior to pooling of the barcoded libraries. The pooled libraries were loaded on the Illumina HiSeq2500 platform and analyzed by a 50 cycles high-output run. Computational analyses were done with the R-based Bioconductor computing environment. FASTQ files were aligned to the mm10 mouse reference genome using the RSubread aligner package (Liao et al., 2013). To adjust the alignment procedure to 3′mRNA-Seq data, the Rsubread align function was executed without trimming but allowing for mismatches in the initial cycles. Only reads with at least 45 bases in length were included in the analysis. Initial mapping with the Rsubread algorithm ('align') was done with a relaxed setting allowing for ambiguous mapping (max two genomic sites to allow for junction reads), but gene level summary with the 'featureCounts' methods was set to unique mapping. The voom method of the limma package was used for normalization and linear modeling (Law et al., 2014). The mRNA expression values were transformed to log2 values of read counts per million (log2 cpm). Differential expression analyses were done using the limma functions 'lmFit', 'eBayes' (eBayes moderated t test statistics) and 'topTable'. The contrast design is outlined in the respective figure panels, legends and main text. Other Bioconductor and R packages used for the analyses and data visualization include (as listed in the key resource table): edgeR, org.Mm.eg.db and heatmap.3 (with modifications), beeswarm.

Gene set enrichment analysis

The java-based stand-alone version of the Broad Institute GSEA software was downloaded from https://www.gsea-msigdb.org/gsea/index.jsp. For the analysis, the t test statistics values (eBayes moderated t test statistics) were used as ranked metrics for the pre-ranked gene list algorithm of the GSEA algorithm with 1000 perturbations (Subramanian et al., 2005). The hallmark gene set collection of the Molecular Signature database (MSigDb) was used (Liberzon et al., 2015) and complemented with melanoma phenotype signatures ('invasive', 'proliferative') (Verfaillie et al., 2015).

QUANTIFICATION AND STATISTICAL ANALYSIS

Statistical analyses

Statistical significance of experimental results was evaluated with GraphPad Prism 8 software using the parametric unpaired two-tailed student's t test, non-parametric Mann-Whitney-U test, log-rank test depending of the type of source data. P values less than 0.05 were considered as statistically significant. Raw p values were corrected for multiple comparisons if required using the Benjamini & Hochberg (B&H) methods (false discovery rate, FDR).

Selection of statistical tests

Tumor area was considered as normally distributed values with similar variances. Parametric tests (t test) were used for significance analysis in these cases. Frequencies of cell populations (percentages) determined by flow cytometry were compared with non-parametric Mann-Whitney test as well as parametric t tests after reciprocal transformation. 3′mRNA-Seq gene expression data were considered as normally distributed after voom normalization and linear modeling allowing for parametric statistical tests and other methods requiring normal distribution of data (Law et al., 2014). Survival probabilities with 95%-CI were calculated according to Kaplan-Meier and compared with long-rank test statistics. The statistical tests were performed with the GraphPad Prism 8 software or the R computing platform. Applied statistical test are specified in the respective figure legends including direction (e.g., unpaired two-tailed Student's t test).